Rigo, T., and N. Pineda, 2016: Inferring the severity of a multicell thunderstorm evolving to supercell, by means of radar and total lightning. *Electronic J. Severe Storms Meteor.*, **11** (2), 1–27.

Electronic Journal of
SEVERE STORMS METEOROLOGY

Inferring the Severity of a Multicell Thunderstorm Evolving to Supercell, by Means of Radar and Total Lightning

TOMEU RIGO AND NICOLAU PINEDA
Servei Meteorològic de Catalunya, Barcelona, Spain

(Submitted 6 July 2014; resubmitted 19 September 2015; in final form 22 March 2016)

ABSTRACT

This study analyzes a long-lived thunderstorm with supercell characteristics that took place in the northeastern Iberian Peninsula on 5 July 2012. Severe weather features identified in Doppler radar and total lightning data have been used to infer the severity of this large-hail-bearing storm that substantially damaged local agriculture. Key elements identified in the radar product analysis were: relatively short development time, a long mature phase lasting >2 h, and high and sustained values for most of the radar parameters (reflectivity, vertically integrated liquid, echo tops), which showed an evolution from multicell to supercell structure. Nevertheless, the most significant patterns were the vertical lifting of the cell core, the three-body scatter spike, the bounded weak-echo region, and the anticyclonic rotation, observed in the Doppler velocity fields. Key features identified in the lightning analysis were: 1) the total lightning "jump" as an early sign for severity, 2) the low negative cloud-to-ground (CG) flash rate and 3) the low intensities in negative CG strokes and the regular rate of positive CG as indicators of complexity in the electrical structure. Finally, data strongly suggest the worst damage occurred when the thunderstorm was in its supercell stage. This case study presents one of the first documented supercells in the region.

1. Introduction

Hail events are quite frequent in Catalonia (northeast part of the Iberian Peninsula). Although hailstone diameters typically range from 5–20 mm, some severe events hit the region almost every year, bearing hailstones up to 50 mm. Other adverse phenomena are often observed in these cases, such as strong winds, high lightning rates and large rain intensities (e.g. Pascual 2002; Pineda et al. 2009).

Literature reveals that other storms in this region have presented supercellular patterns, although the reviewed studies did not make explicit remarks on this condition (Aran et al. 2009; Bech et al. 2009; Bech et al. 2011; Gayà et al. 2011; Bech et al. 2007; Ramis et al. 1997; Pineda et al. 2011).

Corresponding author address: Tomeu Rigo, Servei Meteorològic de Catalunya, carrer Berlín 38 Barcelona 08029, Spain.
E-mail: tomeur@meteo.cat

The region of interest (hereafter, ROI) is locally known as the Plain of Lleida (Fig. 1). Its geographical configuration, described in the next section, makes it prone to suffer hail episodes each year (in general, between two and five relevant hail events). As the area bases its economy on agriculture, the important economic losses caused by hail every year led to a monitoring effort by means of a hail-pad network, automatic weather stations, and trained field observers.

The study of the hail impacts in the ROI has been approached from a variety of perspectives, ranging from diagnosis (e.g. remote sensing, NWP) to climatology and case-study analysis. Some work dealt with the application of methodologies for hail identification and diagnosis, looking for common features in a list of events. For example, Ceperuelo et al. (2009) pointed out that the maximum onset of convection usually coincides with the time of

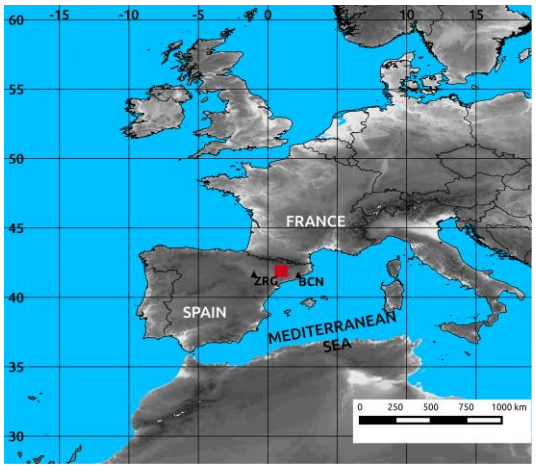

Figure 1: Area of study (red square) within western Europe. Black triangles show the position of nearby rawinsonde stations (Zaragoza, ZRG, and Barcelona, BCN). *Click image to enlarge.*

maximum radiance, which at the beginning of July is at 1200 UTC in the ROI. They also observed correlations between hail and radar parameters, using principal-component analysis. López and Sánchez (2009) made an equivalent work, using discriminant analysis instead. Both studies concluded that the most relevant parameters to infer hail presence are a combination of many of the radar magnitudes, such as reflectivity at surface, the height of the reflectivity echoes, and the maximum reflectivity. Other analyses compare hail parameterization with radar variables (e.g. Fraile et al. 2001). To sum up, these works reveal that automatic hail discrimination techniques need other inputs apart from radar data. Other papers focus on the analysis of the thermodynamic structure enabling hail formation (Aran et al. 2007; Palencia et al. 2010).

Palencia et al. (2010) linked the degree of representativeness of a sounding to its temporal and spatial proximity to the region of concern. Two soundings are launched daily (0000 and 1200 UTC) close to the ROI (Fig. 1). Zaragoza is 195 km west of the ROI, while Barcelona is 150 km to the east. Aran et al. (2007) found that the degree of representativeness of these two radiosoundings, for the present ROI, depend on the meteorological situation, Zaragoza being more representative for hail conditions.

In terms of climate analysis, there are studies focusing on the observation and classification of convection patterns in the Ebro Valley (Fig. 2) (García-Ortega et al. 2011; Aran et al. 2011). Other related works carried out meteorological analysis of significant hail episodes in the ROI (Pineda et al. 2009; Ceperuelo et al. 2006; Montanyà et al. 2009). The first one analyzed the hailstorm of 17 September 2009, where hail stones reached 50 mm. This storm presented features that can be associated to supercellular convection (V-shape in infrared satellite imagery, or some evidence of rotation in the Doppler radar velocity images), but the authors do not provide a detailed analysis on this aspect. Another main event identified in the review was Ceperuelo et al. (2006). Hail reported on their 11 September 2004 episode reached diameters around 3 cm. There was some evidence of a supercell embedded into a group of cells, but this aspect was not further developed by the authors. Most of the significant radar parameters exhibited elevated and persistent values. Finally, a third example of a severe hailstorm in the ROI was analyzed by Montanyà et al. (2009). Contrary to the previous works, this analysis relies on total lightning, revealing the possibility of a complex structure, based on the predominance of positive cloud-to-ground flashes (hereafter, CG). However, like the previous cases, there is insufficient evidence to state that convection reached supercellular mode.

The study of severe weather events enhances the warning-decision-making process, and such studies are crucial for gaining the most benefit from remote sensing technologies. The correct and quick interpretation of available radar and lightning data is key to inferring thunderstorm severity during weather surveillance. As each remotely sensed data source provides only a partial picture of the storm, the combination of the available data enhances its usefulness. It is crucial to identify the severe weather threats among the large number of thunderstorms that develop during the warm season.

The present work presents the analysis, mainly through radar and lightning observations, of an exceptional hailstorm, with some supercell signatures, that produced large hail (up to 7 cm) and important economic losses in agriculture. The main aim of this paper is to improve the short-term forecasting of severe convective weather in the Mediterranean area through the analysis of relevant case studies such as the present one. Secondary objectives are to: 1) identify features related to severe weather, 2)

provide evidence of the presence of a supercell in the stage where more damage was produced, and 3) describe the key elements that may help to discriminate between exceptional severe large-hail storms and frequent small-sized hailstorms.

Data and methods are presented in section 2. Section 3 presents the analysis of the episode. The evidence for a supercell is examined in section 4. Finally, conclusions are presented in section 5.

2. Data and methodology

a. Study area

The ROI is part of the Lleida Plain, an agricultural area about 382 000 ha that comprises basically orchards (e.g. apples, pears, peaches, almonds) and sweet-corn fields. The Lleida Plain (200–400 m MSL) is located in the final section of the Ebro basin, a triangular shaped valley, ca. 400 km long, closed in by important mountain ranges (Pyrenees, Iberian System). The stepped slopes of the Montsec range clearly delimit the north boundary of the Plain (Fig. 2). To the south, the Ebro River flows through narrow gorges to the Mediterranean Sea. The Pre-Coastal Catalan Mountains, a moderate-elevation mountain range (500–1000 m MSL) southeasterly delimits the ROI, while the Ebro basin bucket extends to the west. As a consequence of this geographic configuration, most of the severe thunderstorms hitting the ROI arrive from the SW in a mature stage, having grown in the hillsides of the Iberian System.

b. Weather stations and hail pads

There are 32 automatic weather stations (AWS) in the ROI, corresponding to the network of AWS managed by the Servei Meteorològic de Catalunya (Meteorological Service of Catalonia, SMC hereafter). This network provides data each 30 min for many weather variables (e.g. rain rate, solar radiation, temperature, humidity, wind speed and direction). Also, a hail-pad network has been deployed in the ROI in order to study hail impacts in the area (Aran et al. 2007). This facility is composed of 170 hail pads (Fig. 2), with a nearly regular distribution mesh of ≈ 4 × 4 km.

c. Weather radar network (XRAD)

The main source of information available for this study comes from the remote-sensing systems of the SMC. The primary tool is the weather radar network (XRAD) composed of four radars (Fig. 2). In the present study the two closest radars were La Panadella-CDV (41.602N, 1.403E; 825 m MSL) located ≈50 km east of the ROI and Llaberia-Tivissa-LMI (41.092N, 0.863E; 925 m MSL), 60 km south. The XRAD radars operate in C-band (5.600–5.650 MHz) and are single-polarization Doppler type. All radar displays used in this paper have been generated by commercial software implemented in the radar network (Interactive Radar Information System, IRIS; Vaisala 2014).

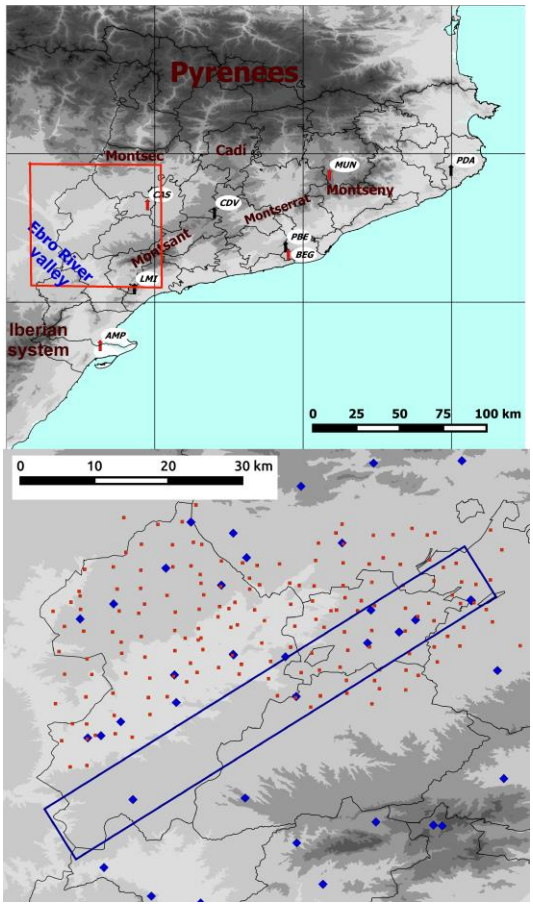

Figure 2: Top: Catalonia, in the northeast part of the Iberian Peninsula. Locations of the SMC Radar network (XRAD) are labeled PDA, PBE, CDV, and LMI. The four SMC lightning dectectors are labeled CAS, MUN, BEG, and AMP. Relevant mountain ranges (dark red) are labeled, as well as the Ebro River valley. A red rectangle delimits the Plain of Lleida (ROI). Bottom: zoom on the ROI, showing the automatic weather stations (blue diamonds) and hail pads (red squares). *Click image to enlarge.*

For the current case study, radar data presented good quality and the possible intrinsic errors of the radar have been discarded. The comparison of the quantitative precipitation estimation (QPE) of the radar versus the SMC rain gauges network presented acceptable bias (between –0.86 and –1.24, within the range of optimal values for the XRAD in summer). As mentioned in Yang and King (2010), C-Band radars are very susceptible to signal attenuation, and in the case of hail events, signal blockage. In the XRAD, these negative effects are partially mitigated using a composite of all the radars, which are in relatively close proximity, and distributed in order to produce a good coverage over the area of Catalonia. In fact, 96% of the whole Catalan territory is covered by at least one volumetric raw, while 58% is covered by the 3D scan of two or more radars. The current ROI is entirely covered by two radars (LMI and CDV). Notwithstanding the above, unfolding problems have been observed in data velocity for the current case study, the unambiguous velocity being fairly low. Furthermore, velocity data contains many contaminated pixels, associated with the filters configuration of the raw files, the strong shear in the region, and the dual PRF technique.

d. Total-lightning location system

In addition to the radar network, the SMC operates a lightning location system (LLS) covering Catalonia with four Vaisala LS-8000 detectors. Intracloud (IC) and CG flashes are detected and processed separately by the system. On one hand, IC flashes are detected in the 110–118 MHz VHF band and located using interferometry (Lojou and Cummins 2006). The combination of the four different concurrent observations provides two-dimensional location of the VHF sources, as the baseline (135–150 km) of the LS-8000 does not allow three-dimensional location (Lojou et al. 2009). The LLS is able to locate a maximum of 100 s^{-1} detections in windows of 100-μs time resolution. Each VHF source is classified as part of an IC flash or, as an isolated IC source (also known as "singleton"; Williams et al. 1999), on the basis of spatial and temporal criteria. Two successive VHF sources are associated in the same IC flash if spatial and temporal intervals between them are lower than 10 km and 0.5s, respectively. Singletons are not included in the IC flash counts in the present case study, seeking not to overestimate total lightning-flash rates.

On the other hand, CG return strokes are detected by a low frequency (LF) sensor and located using a combination of the TOA/MDF (time-of-arrival/magnetic direction finding) technique (Cummins et al. 1998). CG strokes are grouped into CG flashes using an algorithm based on a time and distance criterion. The algorithm allows a maximum inter-stroke interval of 0.5 s and a maximum flash duration of 1 s. The flash spatial radius is limited to 10 km (Cummins et al. 1998). Total lightning hereafter is the sum of IC and CG flashes.

Throughout the years of operation, the LLS performance has been evaluated experimentally by means of electromagnetic field measurements and video recordings of natural lightning in successive campaigns (Montanyà et al. 2006; Pineda and Montanyà, 2009; Montanyà et al. 2012). Additionally, since 2011 data from a Lightning Mapping Array (van der Velde and Montanyà 2013). Those operating in the area of coverage of the LLS have been used to establish the intra-cloud detection efficiency (DE) of the LLS. The analysis of the 2013 campaign establishes a CG flash DE for the LLS around 80–85% and an IC flash DE around 70–75%. The estimated median location accuracy of the LLS for the CG strokes is ~1 km.

3. Analysis of the episode

a. Atmospheric conditions and initial background (1200–1500 UTC)

The synoptic pattern at 1200 UTC 5 July 2012 was marked by a deep middle–upper-tropospheric low over western France, which produced an advection of potential vorticity (PV) (dark band that reached the central part of the Iberian Peninsula in Fig. 3). The trough had an orientation from north to south, which is a quite frequent situation associated with hailstorms in the studied area (Aran et al. 2011; Pascual 2002). The red lines show the height of 1.5 PVU. The maximum values, coincident with the Atlantic low, indicate the anomaly of the tropopause dynamics. The conditions associated with this anomaly had induced ascending motion ahead, affecting the NE of the Iberian Peninsula. The potential-vorticity advection was accompanied by a jetstream with a maximum placed at the NW of Spain. This situation had favored the vertical motion in the upper troposphere, which is one of the elements for the development of the process known as deep convection (Doswell et

al. 1996; Brooks et al. 2003). However, two other factors are necessary in the lower levels: the presence of warm and moist air, as well as some mechanism to lift this air mass.

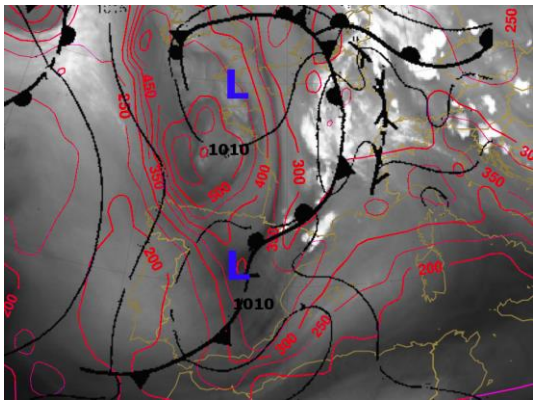

Figure 3: Water-vapor satellite (6.2-μ channel) of the MSG at 1200 UTC, including PV isopleths equaling 1.5 PVU (red lines, hPa), and the surface fronts (black) (provided by EUMeTrain: http://eumetrain.org/). *Click image to enlarge.*

Surface cyclogenesis occurred on 4 July 2012 in the center of the Iberian Peninsula, over the western part of the Ebro Valley. Although it was not a deep low, when combined with a translation to the southeastern part of Spain, it was able to modify the winds at low levels, causing southeasterlies at 1200 UTC, veering to southerly at 1500 UTC (Fig. 4). These winds advected warm and humid air over Catalonia. This in turn increased potential instability in the ROI and surroundings. Importantly, a shortwave trough is evident in the Meteosat water-vapor imagery. The trough located in the center of the Iberian Peninsula helped to support convection in the southern part of the Pyrenees during the morning.

The skew *T*–log*p* diagram from the radiosonde data at 1200 UTC yielded values of surface-based CAPE of 418 J kg^{-1} in Barcelona and 125 J kg^{-1} in Zaragoza (BCN and ZGZ in Fig. 1, respectively). Other thermodynamic values derived from the soundings of BCN and ZGZ are presented in Table 1. Similar values were reported in previous hail events in Catalonia (Tudurí et al. 2003; Ceperuelo et al. 2006; Aran et al. 2007; Pineda et al. 2011). As commented before, the degree of convection was not supercellular in any of those episodes. Furthermore, the thermodynamic values did not seem conducive for the development of supercellular convection. For these reasons, the thermodynamic conditions in the region of initialization of the studied cell were simulated.

A Weather Research and Forecast (WRF) model sounding was based on values at low levels (surface to 810 hPa) in the region where the initial convective element (hereafter "cell #1") started. The simulation was generated for 1500 UTC. The WRF (version 3.1.1; Skamarock et al. 2008) parameterization was as follows: 3-km grid spacing, Yonsei University (Hong et al. 2006) verson 2.2 boundary-layer scheme, Thompson 3.0 (Thompson et al. 2004, 2008) for cloud microphysics, Kain-Fritsch (Kain 2004) for convection, Rapid Radiative Transfer Model (Mlawer et al. 1997) for longwave radiation, Dudhia shortwave radiation (Dudhia and Moncrieff 1989), and Noah land-surface (Ek et al. 2003).

On the other hand, the average values of the Zaragoza and Barcelona soundings at 1200 UTC were used for the mid and higher levels of the atmosphere (Fig. 5). CAPE obtained in the area ahead of convective structure by the simulated sounding at 1500 UTC was 692 J kg^{-1}. This moderate value of CAPE was combined with a convergence line, which was produced by the interaction of the breeze that reached the ROI by the different valleys (mainly the Ebro Valley), and a northwest wind (Fig. 4). The convective structure affecting the ROI 2 h later developed over this line.

Although some thunderstorms already had affected the ROI in previous hours, it was not until 1200 UTC (1400 LST) when deep convection started in the Ebro Valley, near the Iberian System (Fig. 2). Summer convection in the region generally starts later, between 1300 and 1400 UTC (Pascual 2002; Rigo et al. 2008). Thus, the earlier initiation of strong convection in the current event indicates unusually strong instability.

With time, the disorganized cluster of convective cells became more active, reaching higher vertical developments. Another factor is the strong midday insolation, with values measured by the AWS of the SMC of global solar irradiance of 900–1100 W m^{-2}, which supported very deep convection. Temperatures increased to ≈30 ºC in the Ebro Valley at 1330 UTC, along with a decrease of the dewpoint and

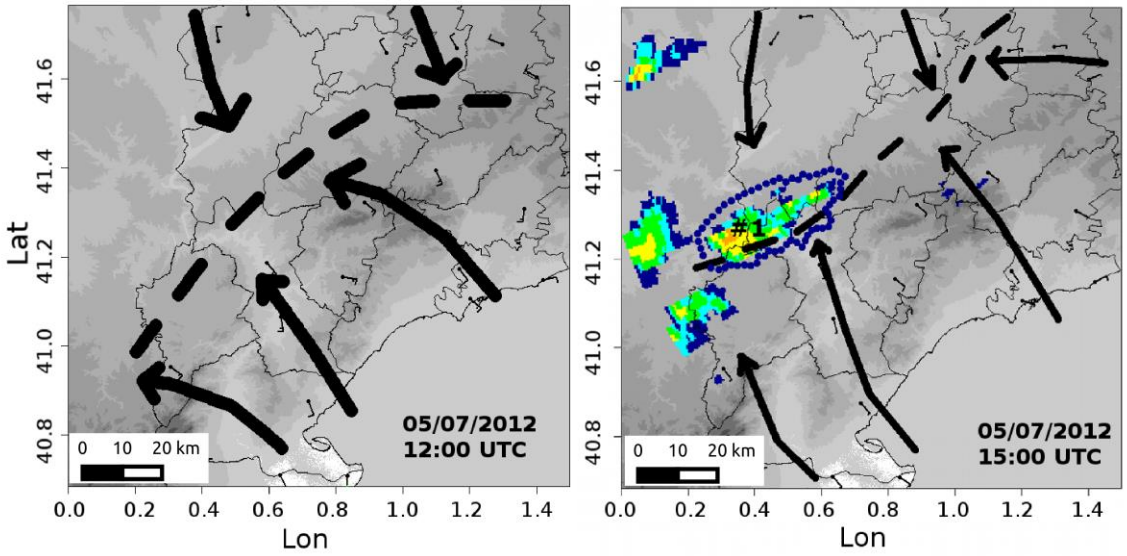

Figure 4: Wind observations from AWS at 1200 (left) and 1500 UTC (right). Thick arrows indicate the mean direction of wind; the dashed line represents the convergence axis. 3-km constant-altitude plan-position indicator (CAPPI) from CDV radar shows the initial position of the main cell (surrounded by a dotted blue line). *Click image to enlarge.*

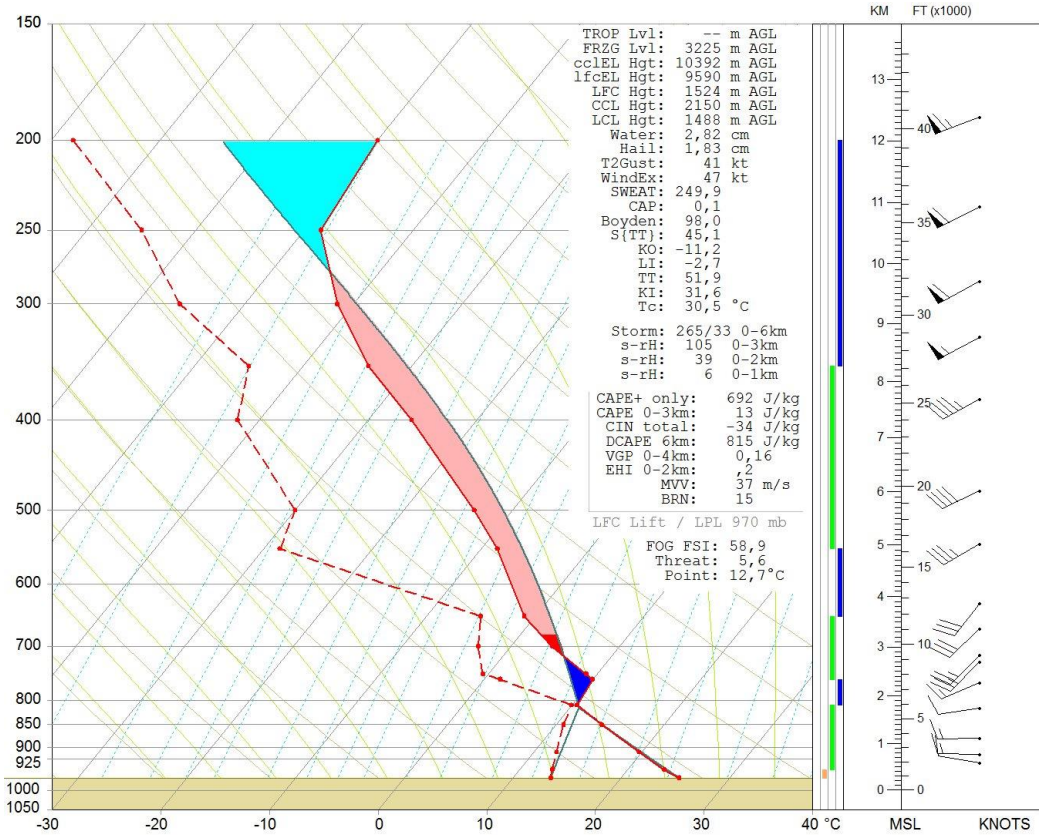

Figure 5: WRF simulated sounding in skew T–log*p* form, corresponding to area ahead of cell #1 at 1500 UTC 5 July 2012 (see text for details). *Click image to enlarge.*

pressure. Around 1430 UTC, convection intensified in the area of the Ebro Valley, with new cells developing in apparent response to the sea breeze interaction with the wind going down through the Ebro Valley (Fig. 6). The cell of interest (hereafter cell #1) formed in front of the disorganized cluster of convective cells.

Table 1: Most relevant non-CAPE thermodynamic indices from the Barcelona (BCN) and Zaragoza (ZRG) soundings at 1200 UTC 5 July 2012.

INDEX	BCN	ZRG
LI (Lifted Index, °C)	−1.2	0.3
TT (Total Totals)	48.2	48.2
K Index	27.3	31.1
SWEAT	171.2	158.6

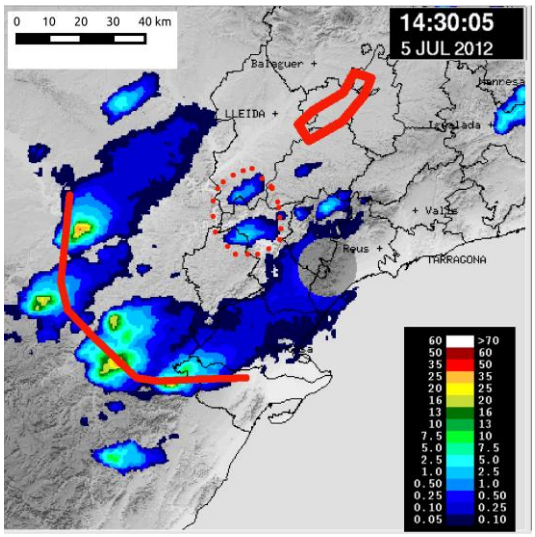

Figure 6: Thunderstorm configuration at 1430 UTC (before the formation of the main cells described in this paper), from VIL field of the LMI radar. Red lines refer to the first cluster of convective cells (solid), the zone of new development of convection (dotted), and the large hail affected area (wide solid line). *Click image to enlarge.*

b. Life cycle of cell #1 (1500–1800 UTC)

First radar echoes from cell #1 were detected in the 1448 UTC image, southwest of the ROI. In a short while, intense reflectivity values were observed at low and midlevels as well as moderate vertically integrated liquid (VIL) values (>30 mm) (1448–1530 UTC) (Fig. 7). According to Edwards and Thompson (1998), moderate VIL indicates small-to-moderate hail. First lightning was detected in cell #1 at 1448 UTC, corresponding to VHF bursts related to IC activity. The first CG, a negative single stroke of –9 kA was detected 10 min later. From 1500 UTC on, cell #1 moved relatively fast (30 km/h average speed), to the northeast (Fig. 8), and produced small hail. Some damage was reported in agricultural areas, with maximum hail diameter close to 20 mm. From 1430–1530 UTC, the more remarkable features observed on the AWS of the SMC were: an hourly maximum precipitation rate near 25 mm, wind direction veering to northerly as a consequence of the entrance of the breeze in the region, an average decrease in surface temperature of 4ºC, and a dewpoint increase of 2ºC.

After 1530 UTC cell #1 began to stand out from the rest of cells as it changed course, veering 30° to the left of the general motion direction (Fig. 8). During this first stage, the cell had a multicellular aspect, with some new developments in its rear flank. Figure 7 shows how the total lightning flash rate (TFR) increased steeply in a 50-min period, reaching its absolute maximum at 1540 UTC, ≈1 h after the first IC signals detected in the cell, reaching 70 min^{-1}, and between 8 and 10 CGs min^{-1}. After this maximum, the TFR steadily diminished, sharpening its decline until the later maturity, when the TFR remained rather constant. From 1510–1550 UTC, the echo cores of reflectivity were located at mid-levels (4–8 km) (Fig. 9), coinciding with the period of largest electrical activity. These observations suggest a multicellular behavior during this period.

Another aspect to highlight from Fig. 7 is the similar trend shown by the TFR and the LA-30 (the area of the CAPPI of 7 km exceeding the 30 dB*Z* threshold, also known as the Larsen Area, from Larsen and Stansbury 1974), in line with the findings by Mosier et al. (2011) and Pineda et al. (2011). According to Deierling et al. (2005), the higher the updraft speed, the higher the diffuse threshold will extend. Furthermore, the upper limit has often been associated with radar echo tops corresponding to a reflectivity of around 30 dB*Z*. Thus, the LA-30, which considers the amount of precipitation aloft, relates better to the total lightning activity than simpler parameters like storm height. Williams et al. (1989) observed that the peak of the TFR generally occurs prior to the time of maximum vertical extent of the LA-30; however, in the

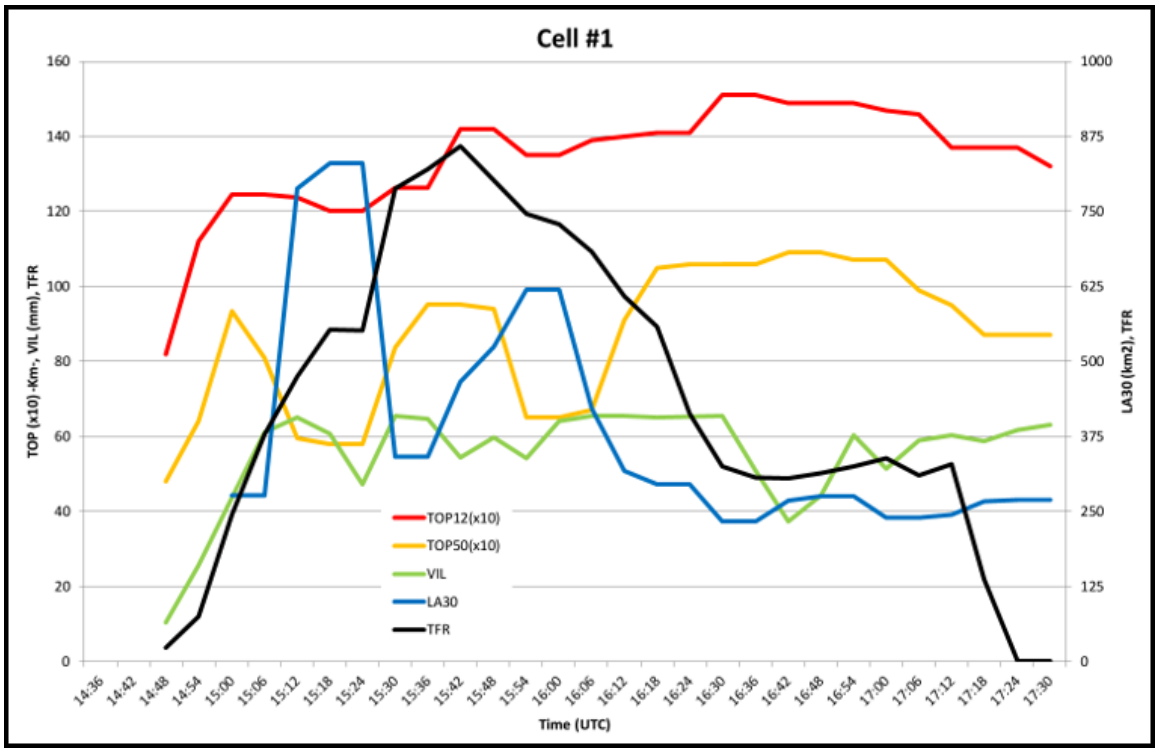

Figure 7: Time series plot of total lightning flash rate, TFR (black), TOP-50 (yellow), TOP-12 (red), VIL (green), and LA-30 (blue) of the life cycle period of cell #1. *Click image to enlarge.*

present case, the LA-30 and TFR reached relative maxima at a similar time. After a fast growth, both parameters reached their maxima quite early (1542 UTC, just 40 min after the onset), considering that the thunderstorm had a long duration. According to Emersic et al. (2011), a scenario of wet graupel growth could explain this situation.

Regarding the CG activity, peak currents of the negative strokes were rather low during the whole episode. The average intensity of the negative discharges for cell #1 was –8.2 kA, the 30th percentile compared to the average for Catalonia (–18.6 kA for the period 2010–2013). On the contrary, average values of positive CG strokes (29.4 kA) were similar to the Catalonian average (29.3 kA). Figure 10 shows the constant-altitude plan-position indicator (CAPPI) product for mid-levels at 1530 UTC for the LMI radar. In accordance with the LA-30 parameter, the 7-km reflectivity exceeded 50 dBZ for an area of ≈50 km^2. This large area of high values at mid–high altitudes indicates deep, moist convection (Doswell et al. 1996). Besides, a multicellular pattern was present around cell #1, showing several areas of moderate reflectivity close to the main updraft (Fig. 8).

Coinciding with the end of the second LA-30 maximum (Fig. 7), a long period showing sustained high reflectivity held aloft began (1610-1710 UTC), indicating a persistent strong updraft and, probably a supercellular behavior (Bunkers et al. 2006a). A similar transition from a multicell to a supercell behavior was analyzed in Vasiloff et al. (1986). The authors suggested that a continuum of thunderstorm types is possible, being unnecessary to dichotomize storms as either multicell or supercell.

On the other hand, parameters such as TOP-50 (echo tops for the 50-dBZ threshold; Lakshmanan et al. 2013) and VIL presented a trend opposite to that of LA-30 and TFR, acquiring their maximum values just when LA-30 and TFR started their decrease. According to Wiens et al. (2005), the electrical behavior (represented by the TFR) is temporally well–correlated with the updraft (w >10 m s^{-1}), but less correlated with the hail-echo volume.

In our case (Fig. 8), the mature period showed high and sustained VIL and TOP-50 values, while the TRF diminished to the lowest values of the life cycle. This decrease in the frequency of IC flashes also was observed by

Montanyà et al. (2007, 2009), who analyzed some hailstorms in the same region. Moreover, +CG activity remained rather constant during the whole mature phase, while the –CG rate decreased by half during this stage, also showing lower peak currents.

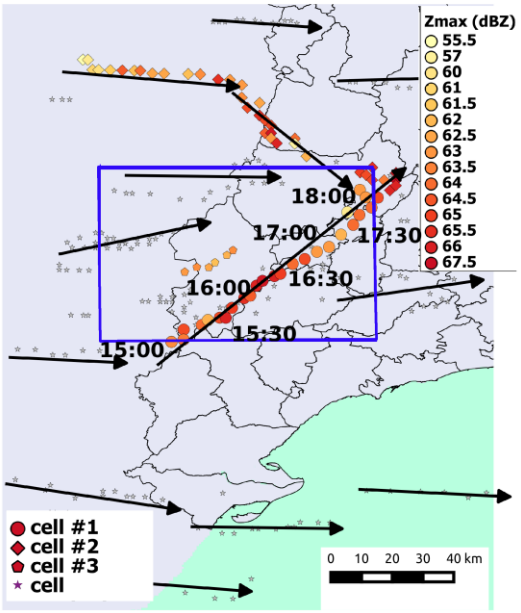

Figure 8: Map of the cell motions, inferred from the calculated centroids (stars) observed in the ROI and surroundings during the 5th July 2012. Main cells are marked with circle (cell #1), diamond (#2), and pentagon (#3). Arrows indicate the direction of each thunderstorm. The times are referred to the cell #1 position. *Click image to enlarge.*

To sum up, the multicellular stage was dominated by the maximum values of TFR and LA-30 along the life cycle, while VIL, TOP-12 and TOP-50 reached some relative maxima, but far off the absolute maxima. Furthermore, the cores of reflectivity were located at midlevels. On the contrary, the supercellular stage was marked by the negative ratio of TFR and LA-30, while VIL, TOP-12 and TOP-50 were increasing until reaching their maxima, coinciding with the period where the core of reflectivity extended in the 1–8-km layer. During the last part of the supercellular phase, between 1630 and 1710 UTC, cell #1 crossed the large-hail-affected area (hereafter LHAA), an area mainly covered with orchards. VIL reached 65 mm (the maximum value in the software), corresponding to large hail (Edwards and Thompson 1998). At the time of reaching the LHAA, cell #1 presented a strong vertical development (TOP12 to 15 km), apparent tilting associated with the vertical shear and intense reflectivity values at midlevels (>60 dBZ at 9-km AGL.

According to the hail-pad network, the hailstones presented a high variability in size across the swath, with higher diameters (up to 7 cm) in the center of the trajectory and lower values on both sides (Fig. 11). Other phenomena reported by local observers and automatic weather stations were strong winds, especially in the left flank (maximum wind gust up to 70 km h^{-1} registered, but possibly higher because of hail damage to the wind sensor), as well as heavy rain rates (2.9 mm min^{-1}).

At this point, we emphasize that other severe thunderstorms were observed during the episode (Fig. 8), the most remarkable being a hailstorm that crossed the northern border of the Lleida Plain (cell #2). Figure 8 also shows the pathway of a third hailstorm (cell #3) which occurred two hours after cell #1. Hailstones of 2 cm were reported west of the ROI for this third cell.

In addition, Fig. 8 highlights the deviant motion of cell #1, left-moving with respect to the general flow, as well as the change in direction of cell #2. This multicell structure was first canalized by the presence of a mountain range located north (left regarding its motion) and an unstable boundary layer air placed south (right). Afterwards, it shifted to the right, likely due to new cell development along the right-flank downdraft outflow (i.e., discrete propagation, as new cells formed in the unstable air at lower elevations along the storm's gust front).

c. Merging and declining phase (1800–2000 UTC)

The path followed by cells #1 and #2 ended in the merging of both thunderstorms. Although the two were already in a decaying stage, the merging probably accelerated their demise. The merger around 1754 UTC led to intensification of the reflectivity and the vertical development of the new merging cell, but only lasted for 20 min. In fact, the new thunderstorm decayed quite fast, and at 1854 UTC it became diluted in the small line that crossed the northern part of Catalonia, associated to the airmass boundary.

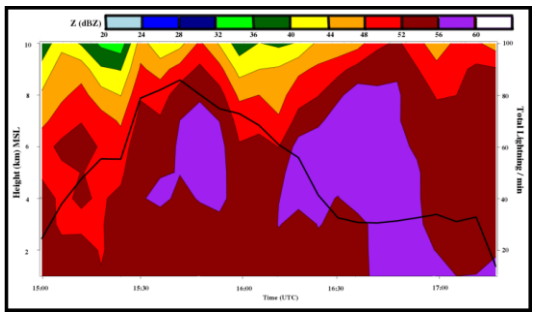

Figure 9: Total lightning flash rate (TFR) evolution per minute (black line) compared with the median reflectivity at different levels for cell #1, 1500–1720 UTC. *Click image to enlarge.*

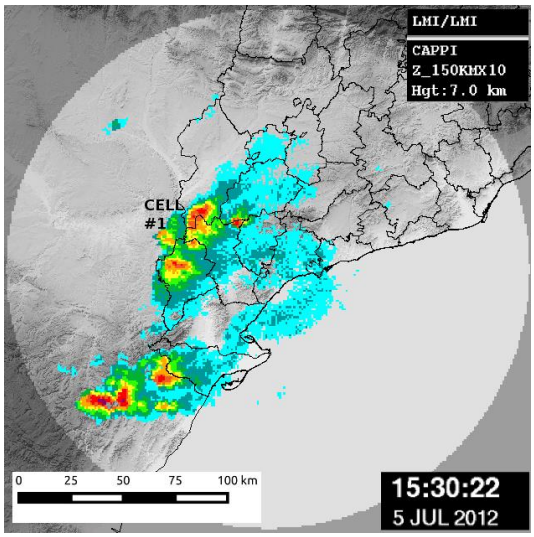

Figure 10: CAPPI at 7 km MSL from LMI radar. *Click image to enlarge.*

4. Evidence of a supercell

This section presents all those elements that have led us to categorize cell #1 as a supercell, at least during a part of its life cycle.

a. Environment

The first question is if the environment favored supercells. As explained above, the meteorological conditions were conducive to deep, moist convection, with high humidity at the surface (the AWS close to the cell #1 gave values of relative humidity close to or >90% between 1530–1730 UTC), a convergence line as a lift source for initiation of convection, and conditional instability (the lapse rate at the region of initiation of the thunderstorm was slightly over 8ºC km^{-1}). In these conditions, the vertical wind profile will determine the type of convection (Doswell 1987).

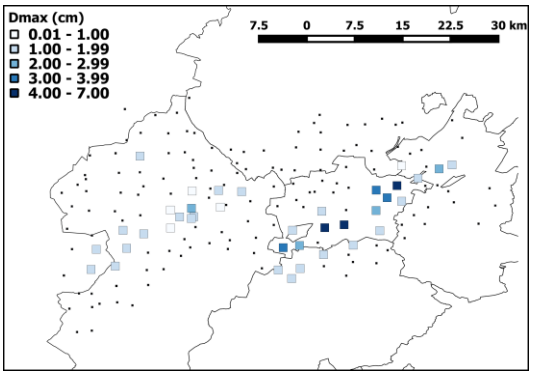

Figure 11: Maximum size of hail measured by the hail-pad network of the ADV. *Click image to enlarge.*

However, the analysis of the wind profile and hodograph showed a favorable environment for severe thunderstorms, but rather marginal for supercells. On the other hand, moderate CAPE values have been reported in supercellular environments (Baker et al. 2009). In any case, another factor must be taken into account: representativeness of the nearby soundings. As Brooks et al. (1994) indicated, to be representative: 1) the storm of interest should be within a 80 km radius from the sounding; 2) it should take place within 105 min after the balloon release; and finally, 3) the air mass that gave birth to the storm should be the same as the one sampled by the sounding. In the present case study, none of these conditions were satisfied by the two nearby soundings. Therefore, in the simulated sounding made over the region, we focus on hodograph analysis.

Values of storm-relative helicity (SRH) were low in all soundings, mainly in the layer 0–1 km (22 m^2 s^{-2}), but also for 0–3 km (<100 m^2 s^{-2}) (e.g., Esterheld and Giuliano 2008; Bunkers 2002; Bunkers et al. 2006b). Furthermore, SRH was probably anticyclonic below the cloud base, thus affecting both the rotation and direction of the storm, as shown in Fig. 12. This figure also shows cell #1's mean storm motion at different periods (A: 1500–1600 UTC, B: 1600–1700 UTC and C: 1700–1800 UTC). It indicates a shifting of the thunderstorm's translation to the left, different from the neighboring thunderstorms. Having in mind that the period in which the anticyclonic rotation of the cell was observed was between roughly 1630–1718 UTC,

this would cause the leftward shift. The speed of the thunderstorm also was increasing during evolution to the supercell stage. That acceleration and the left shift of cell #1 makes SRH more anticyclonic. Therefore, the steering wind in the cloud layer was likely changing toward faster speeds and also perhaps shifting somewhat leftward.

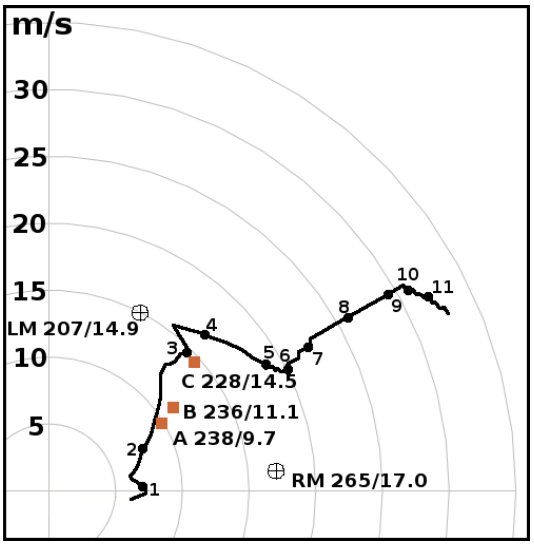

Figure 12: Hodograph from estimated pre-storm environment of Fig 5. The black circles with cross hairs indicate the right and left moving vectors calculated using the Bunkers et al. (2000) technique. The brown squares show the mean storm direction for cell #1 between: a) 1500–1600 UTC, b) 1600–1700 UTC, and c) 1700–1800 UTC. *Click image to enlarge.*

b. Lightning

In terms of the lightning activity, literature indicates that supercells, compared to common thunderstorms, show a complex electrical structure. This complexity refers to a large variability of behaviors. In this sense, they tend to be outliers on a spectrum of electrification intensity metrics, like the TFR, the IC/CG ratio, or the CG polarity (Tessendorf 2009).

Analytic (Blyth et al. 2001) and modeling calculations (Latham et al. 2004) have predicted that the TFR is roughly proportional to the product of the downward mass flux of graupel and the upward mass flux of ice crystals (known as the flux hypothesis). Furthermore, Deierling et al. (2008) provided observations that strongly support the flux hypothesis, reporting a strong correlation between TFR and updraft volume, in particular with vertical velocities >5–10 m s^{-1}. The maximum TFR for supercells may be on the order of 100 min^{-1}, while a common storm typically averages one order of magnitude less (MacGorman et al. 2005). Cell #1 reached a TFR of 86 min^{-1}, whereas typical summer storms in Catalonia average 11 min^{-1} (Rigo et al. 2010).

The TFR for cell #1 also presented an abrupt increase during the development phase, a pattern reported in many severe storms (Williams et al. 1999; Goodman et al. 2005; Wiens et al. 2005; Fehr et al. 2005; Steiger et al. 2007). Williams et al. (1999) called these rapid increases lightning "jumps". Lightning jumps were identified in the present case using the Metzger and Nuss (2013) rule which considers an increase of 10 flashes in a 1-min period, and the increase must be sustained for 3 min. Cell #1 presented two jumps during the growing phase (Fig. 7). In fact, they were only separated by a 5-min gap, thus it may be considered as a unique jump. This jump fits in the "hail-type" category described by Metzger and Nuss (2013), since radar parameters like TOP-50 and VIL showed an increase just after the jump.

Severe storms frequently present dominant positive (+) CG for several tens of minutes during their mature phase (Carey and Rutledge, 1998; Lang et al. 2004; Soula et al. 2004; Wiens et al. 2005). In the case of cell #1, a considerable amount of +CG strikes was recorded in a rather constant rate during two hours (1.7–4.0 +CG min^{-1}). Furthermore, the negative (–) CG flashes exhibit unusual values during the period, with lower peak currents and lower multiplicity values. Cummins et al (2006) noticed that the majority of the low-peak-current (<10 kA) negative discharges in positive-dominant storms were not CGs but ICs with vertically oriented channels. Similar results were obtained by Johnson and Mansell (2006) in a supercell in Oklahoma. In our case study, if we dismiss low peak-current negative strokes (<10 kA) we end with a +CG dominance throughout the whole episode. However, the analysis of this possible positive dominance and the associated charge structure is beyond the scope of the present study.

About the spatial distribution of lightning, the presence of CG strokes in the updraft region was scarce or null. However, a lightning-hole signature (Lang et al. 2004) has not been

observed in the present case. The very large updraft speeds and rotation of the supercell storm made the lowest charge center in the updraft to be higher than usual, producing fewer ground flashes than in a common severe thunderstorm (elevated dipole hypothesis; MacGorman et al. 1989). Later on, CG rates increased as the updraft weakened, related to the downdraft associated with midlevel precipitation. As a general pattern, –CG (>10kA) were closer to the high reflectivity core (>50 dB*Z*), while +CG tended to be related to a lower maximum-reflectivity (30–50 dB*Z*) areas.

Finally, although a peak was recorded in the CG flash rate, the large decrease in the –CG activity, about 18 min prior to the maximum observed hail sizes, can be considered as the main key in surveillance tasks in order to anticipate the hail shaft. The depth of the melting layer plays a fundamental role in the diameter of the hail, as the size of the stones varies rapidly in the last parts of the melting processes (Donavon and Jungbluth 2007). This dependence is not as clear in large hail, because of a minor exposure of hailstone mass to the warm air. For this last type of hail, some evidence exists of a delay of ≈10 min between the collapse of the updraft and the fall out of the storm. This phenomenon also was observed in the present case study, with delays between 12–18 min.

The near-cessation of the CG activity is probably associated with the collapse of the thunderstorm, produced by the large size of hail at mid–top levels of the cell. Another reason may be that hailstones undergoing wet growth may not separate charge in collisions with ice crystals (Saunders and Brooks 1992). In the present case, the maximum total lightning flash ratio (TFR) was registered well before the time of the large-size hailshaft.

c. Key signatures

According to the operational automatic cell-tracking algorithm at the SMC (Rigo and Llasat, 2004; Rigo et al. 2010), cell #1 lasted >3 h (1500–1818 UTC), thus having a long lifecycle. Because the tracking algorithm is rather restrictive when identifying convection, a manual analysis was performed on the lifecycle of cell #1 to describe its duration in detail. Radar imagery showed the first echoes at 1448 UTC, and the last at 1848 UTC. Taking into account that the average duration of convective cells in summer in Catalonia is ≈60 min (Rigo et al 2010), the 4-h duration indicates the strong updrafts of the storm. Moreover, the development stage was quite short, compared to the average development length. In the present case, the development phase was only 12% of the whole lifecycle, compared to the 18% average (Rigo et al 2010).

Regarding the vertical extent of the storm, the most significant feature is the maximum height reached by the TOP-50 (a good indicator of the strong updrafts), with values >11 km for cell #1. The TOP-12 product is used to measure the total height of the thunderstorm. In this case, cell #1 reached a maximum TOP-12 of 15 km (Fig. 7). In this sense, Donavon and Jungbluth (2007) suggested that the main mechanism associated with hail development is an updraft strong enough to maintain growing hailstones at mid–high levels, with sufficient time to attain large diameters. Regarding the horizontal axis, the cell had a maximum longitude of ≈40 km in the parallel direction, and about 30 km perpendicular to the direction of the motion. Keeping in mind the average size of the cells in the area, with 9-km depth (TOP-12) and 7.5 km of radius (Rigo et al. 2010), the values reached by cell #1 were outstanding.

To illustrate the evolution of the size of cell #1, as well as the morphologic changes that occurred throughout its mature phase, Fig. 13 shows the changes in the VIL product between 1624–1654 UTC. The considerable decrease, from >60 mm to 40 mm in 0.5 h, associated with the modification of the vertical pattern of the reflectivity (see also Fig. 9), indicates a change in the dominant updraft. At 1654 UTC, VIL had decreased drastically; implying that the water column collapsed near that time. On the other hand, the size of the cell remained practically constant throughout this period, with an area of >30 mm VILs close to 50 km^2, and an area to 200 km^2 at values >10 mm. However, the size of the cell is not constrained to the limit of 10 mm in the VIL product; 1 mm is a good indicator of the limits of a cell, avoiding considering the stratiform region. Then, the area becomes nearly 650 km^2—more than three times the median regional cell area of ≈200 km^2 (Rigo et al. 2010).

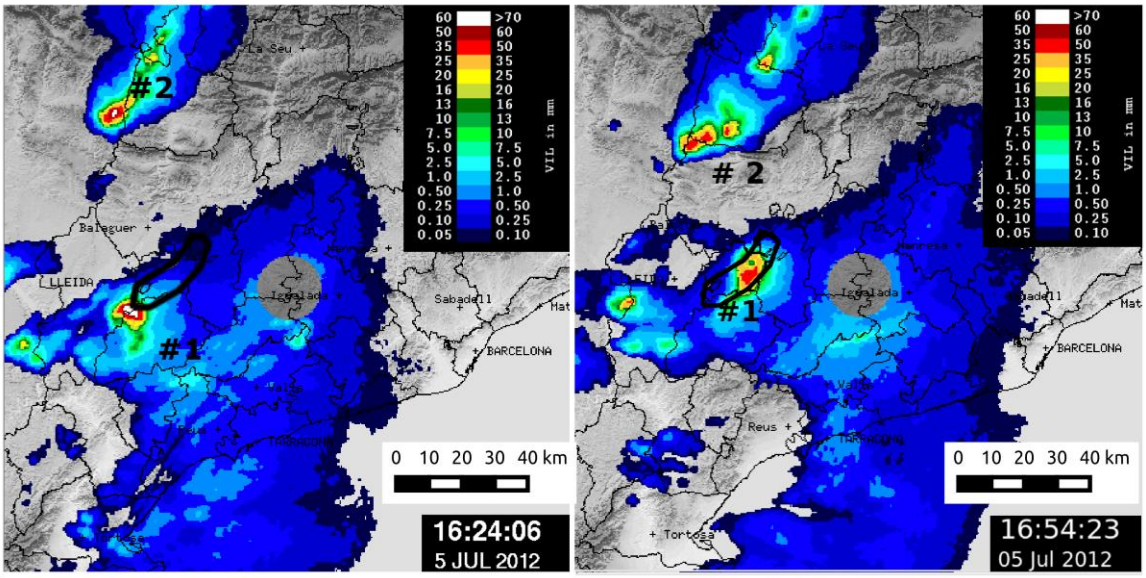

Figure 13: VIL product from CDV radar, at 1624 and 1654 UTC. Cells #1 and #2 are indicated, as well as the LHAA region (black line). *Click image to enlarge.*

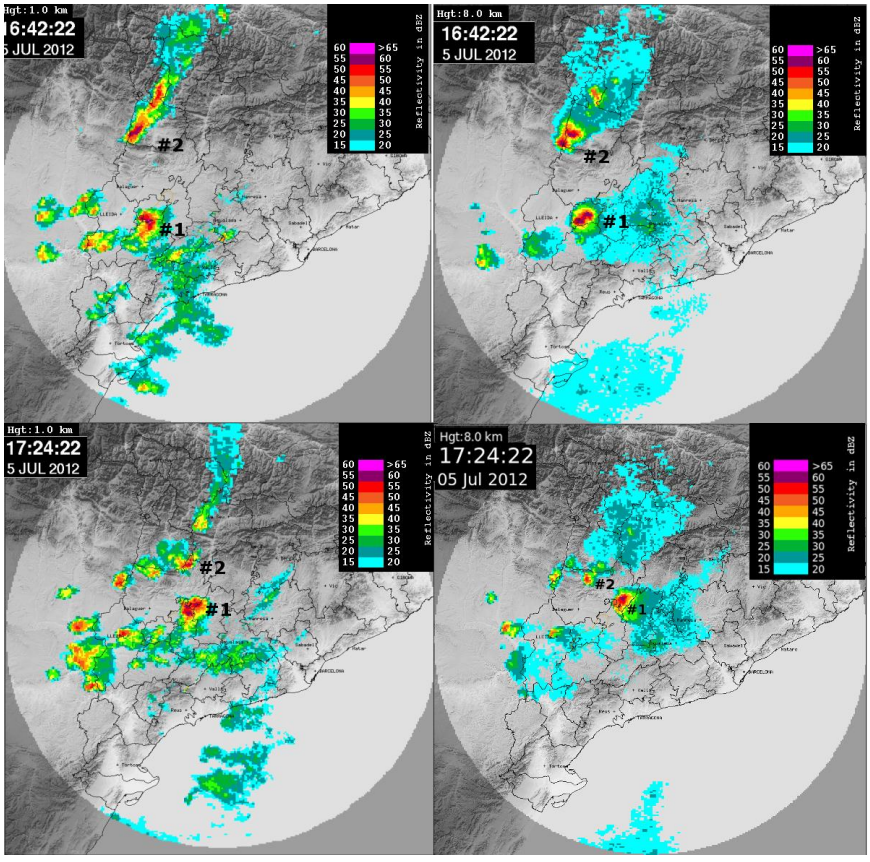

Figure 14: CAPPI at low levels (left) and high levels (right) from the CDV radar at 1642 and 1724 UTC (respectively). Cells #1 and #2 are marked in each chart. *Click image to enlarge.*

Continuing with the analysis of the magnitudes of the thunderstorm, Fig. 14 shows the CAPPI product at low and high altitudes (1 and 8 km AGL, respectively) at 1642 and 1724 UTC. These pictures illustrate the strong updraft of cell #1 compared to cell #2. At 1642 UTC the area with moderate reflectivity was similar in both cells, slightly larger in the cell #2. However, 42 min later, the situation was quite different: while the area of cell #1 had stayed rather constant, cell #2 had been reduced in area by a fifth. Given that both cells initiated almost at the same time, the structure of cell #1 lasted longer. A similar behavior is observed in lower CAPPIs. This difference can be explained by the updraft intensity at the beginning of the lifecycle, and, furthermore by the conditions in which it had grown (high instability, great input of moisture, and the strong surface insolation).

With regard to supercell signatures in the radar reflectivity field, many authors (e.g. Forbes 1981; Fujita 1958; Lemon 1998; Rasmussen and Straka 1998; Bunkers et al. 2006a) refer to the following key patterns: hook echoes, midlevel bounded weak-echo region (BWER), strong reflectivity gradients on the inflow side of the storm, and the three-body scatter spike (TBSS) signature. Figures 15 and 16 present some of these features observed for the cell #1. Except for the hook echo, the other features were identified in the reflectivity fields. Figure 15 illustrates reflectivity features at 1624 UTC. Moreover, a big overhang echo aloft is shown in the left panel, and a small overhang echo aloft in the right panel (Bunkers et al. 2006a; Bruning et al. 2010). The BWER was also observed at 1654 UTC (corresponding to the time of the maximum hailstone size) situated in the left flank, as identified in the cross section of Fig. 15. A leading strong reflectivity gradient can be identified from left-front through right side.

Finally, the TBSS can be inferred at the left of the vertical profile, although it was not especially marked (Fig. 16). In fact, some authors cast doubt on the possibility of detecting the TBSS in C-Band radars. Besides, the same figure also shows a "hail spike" signature, just out the top of the storm. As with the TBSS, it is a large-hail indicator.

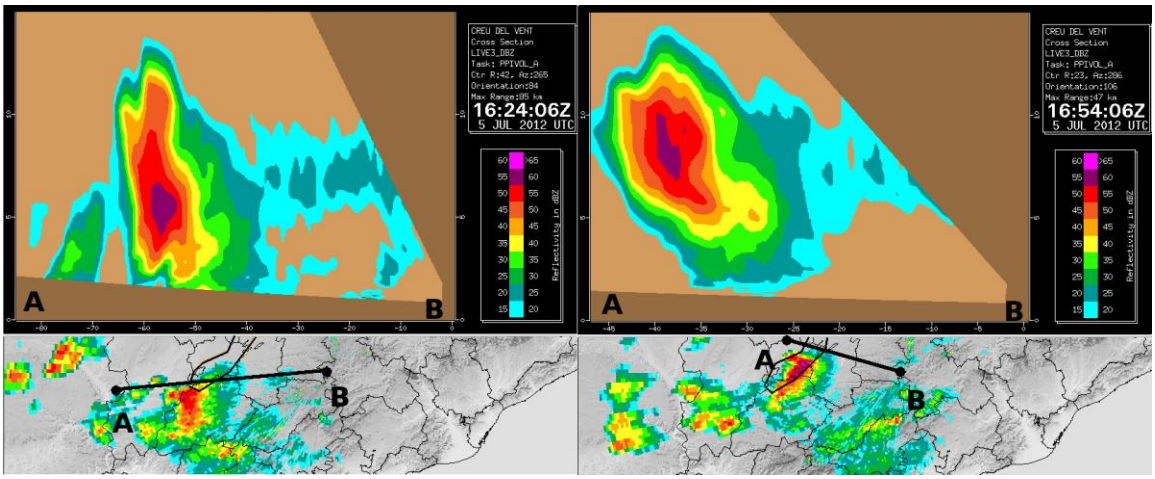

Figure 15: Two reflectivity PPI fields at 0.6º (bottom) and vertical cross sections (top) at 1624 UTC (left), and at 1654 UTC (right), showing the vertical structure of cell #1. *Click image to enlarge.*

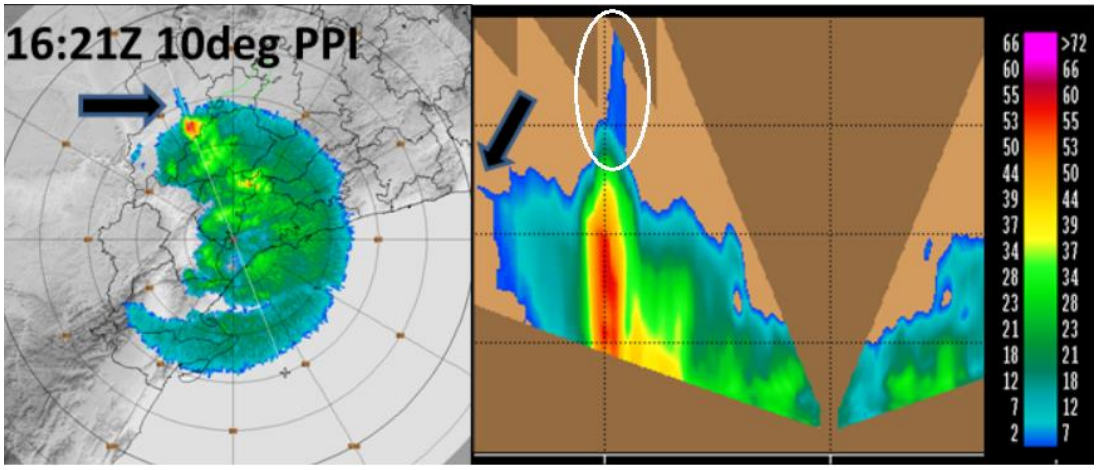

Figure 16: Reflectivity PPI fields at 10º (left), and vertical cross sections (right) at 1612 UTC for cell #1. Black arrows mark the area of the TBSS, while the hail-spike signature is circled. *Click image to enlarge.*

Radar reflectivity and relative wind fields related to supercell-pattern identification are shown in Fig. 17 for both radars at 1654 UTC. The first column shows high-intensity reflectivity echoes well above the melting layer, favoring large-hail formation given the presence of a strong updraft, indicated by the BWER feature shown above (Fig. 16); the X symbol indicates the approximate position of the BWER center. The central column in Fig. 17 shows the presence of strong azimuthal shear at midlevels (3.5–5 km AGL) nearly collocated with the BWER, and more evident in LMI data, suggesting the possible presence of a mesocyclone with anticyclonic rotation (similar patterns can be seen in LMI data from 1638–1702 UTC). This is consistent with the leftward shift shown by the main cell. The third column shows less-definite patterns, suggesting the possible mesocyclone does not extend above 6 km AGL, in agreement with the analysis of higher-angle PPIs. Note here that LMI has a higher-quality Doppler velocity. The presence of the BWER, the high elevated echoes, the azimuthal shear features and the observations of large hail and damaging surface winds are elements suggesting supercellular character.

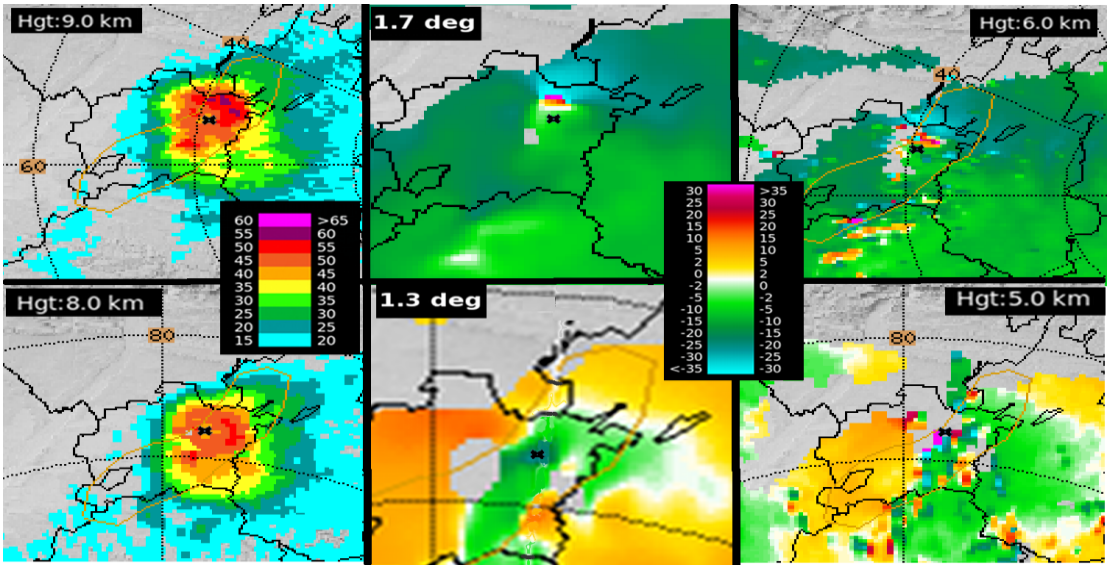

Figure 17: Panel showing different products for CDV (top) and LMI (bottom) radars at 1654 UTC: reflectivity CAPPIs at high levels (left); smoothed velocity PPIs that cross the thunderstorm at midlevels (center); and velocity CAPPIs at midlevels (right). Black X symbols indicate the BWER zone.

5. Summary

This study has analyzed a long-lived thunderstorm that produced large hail and important economic losses in the local agriculture of the Lleida Plain, northeastern Iberian Peninsula. The 70-mm-diameter stones observed that day are, to date, the largest ever reported in the region. Doppler radar and total lightning data have been used to find severe-weather features, seeking to fulfill two objectives: the analysis and categorization of the storm, and to provide new evidence or indicators that can improve the short-term forecasting of severe convective weather in the Mediterranean area.

A synoptic situation favorable for upper-tropospheric vertical motion, along with high humidity and a convergence line at surface had set an auspicious environment for severe thunderstorms. Although the available soundings in the region did not indicate supercellular conditions, these nearby soundings were unrepresentative of the local conditions where the severe storm developed. For this reason, an NWP-simulated sounding has been used to better estimate the local conditions.

With respect to the remote-sensing signatures that could help in warnings, we focus on radar and lightning. For lightning, we stress the lightning jump, the –CG flash rate and CG polarity shifts. The lightning jump is an early sign for severity and highlights the interest of having total-lightning detection available during surveillance. In Catalonia and elsewhere, a low –CG flash rate has been related to the collapse of the main reflectivity core, producing the larger hail. Finally, we emphasize the interest of monitoring the polarity and intensity of the CG strokes. In the present case study, the low intensities in –CGs and the regular rate of +CGs indicated complexity in the electrical structure of the cell and should be considered as indicators of potential severity.

Key elements on radar imagery can be summarized in three main aspects. Firstly, the supercell achieved a large vertical development (above 11 km for the TOP-50) in a short timespan, compared to that of the storm. In general, thunderstorms reach maximum development in the middle of their lifecycle and, after a brief period, start decaying. However, in the present case, the maximum was observed in the first 10% of the whole duration. Secondly and also associated with the storm duration, TOP-50, VIL and reflectivity showed very high and sustained values for >2 h. The two first points are clear indicators of storm severity, evident at the surface with large hailstones and strong wind gusts. High rain rates also were observed. Moreover, the storm evolved along the continuum of classifications from multicell to supercell.

Finally, regarding the identification of supercell-related patterns in radar reflectivity and relative wind fields, it was possible to identify the TBSS signature, as well as the BWER. On the contrary, the identification of a couplet associated with the mesocyclone was more complicated. Still, in an operational environment, there would have been enough signatures to issue a warning for severity. In fact, we think that even without the identification of the reflectivity patterns, a good tracking system of the cell lifecycle, showing information on the evolution of the key radar parameters, could be sufficient to provide clear severity trends to the forecaster. Furthermore, the deviant motion of the main cell indicated of a favorable environment for anticyclonic rotation at low levels.

ACKNOWLEDGMENTS

The authors would like to thank the valuable contributions made by P. Altube, C. Farnell, and J. Bech. Besides, we highly appreciated the critical reviews by Romero and Holle. We are grateful to editor Roger Edwards for his guidance. Special thanks to associate editor Robert Maddox, who made a huge effort which substantially strengthened this paper. We also wish to acknowledge all the people that participated in the gathering of ground evidence of the damages caused by a hailstorm that will be remembered in the region for years.

REFERENCES

Aran, M., A. Sairouni, J. Bech, J. Toda, T. Rigo, J. Cunillera, and, J. Moré, 2007: Pilot project for intensive surveillance of hail events in Terres de Ponent (Lleida). *Atmos. Res.*, **83**, 315–335.

——, J. Amaro, J. Arús, J. Bech, F. Figuerola, M. Gayà, and E. Vilaclara, 2009: Synoptic and mesoscale diagnosis of a tornado event in Castellcir, Catalonia, on 18th October 2006. *Atmos. Res*., **93**, 147–160.

——, J. C. Pena, and, M. Torà, 2011: Atmospheric circulation patterns associated with hail events in Lleida (Catalonia). *Atmos. Res*., **100**, 428–438

Baker, A. K., M. D. Parker, and M. D. Eastin, 2009: Environmental ingredients for supercells and tornadoes within Hurricane Ivan. *Wea. Forecasting*, **24**, 223–244.

Bech, J., R. Pascual, T. Rigo, N. Pineda, J.M., López, J. Arús, and M. Gayà, 2007: An observational study of the 7 September 2005 Barcelona tornado outbreak. *Nat. Hazards Earth Syst. Sci*., **7**, 129–139.

——, M. Gayà, M. Aran, F. Figuerola, J. Amaro, and J. Arús, 2009: Tornado damage analysis of a forest area using site survey observations, radar data and a simple analytical vortex model. *Atmos. Res.*, **93**, 118–130.

——, N. Pineda, T. Rigo, M. Aran, J. Amaro, M. Gayà, J. Arús, J. Montanyà, and O. van der Velde, 2011: A Mediterranean nocturnal heavy rainfall and tornadic event. Part I: Overview, damage survey and radar analysis. *Atmos. Res.*, 1**00**, 621–637.

Blyth, A. M., H. J. Christian Jr., K. Driscoll, A. M. Gadian, and J. Latham, 2001: Determination of ice precipitation rates and thunderstorm anvil ice contents from satellite observations of lightning. *Atmos. Res.*, **59**, 217–229.

Brooks, H. E., C. A. Doswell III, and J. Cooper, 1994: On the environments of tornadic and nontornadic mesocyclones. *Wea. Forecasting*, **9**, 606–618.

——, ——, and M. P. Kay, 2003: Climatological estimates of local daily tornado probability for the United States. *Wea. Forecasting*, **18**, 626–640.

Bruning, E. C., W. D. Rust, D. R. MacGorman, M. I. Biggerstaff, and T. J. Schuur, 2010: Formation of charge structures in a supercell. *Mon. Wea. Rev.*, **138**, 3740–3761.

Bunkers, M. J., 2002: Vertical wind shear associated with left-moving supercells. *Wea. Forecasting*, **17**, 845–855.

——, B. A. Klimowski, J. W. Zeitler, R. L. Thompson, and M. L. Weisman, 2000: Predicting supercell motion using a new hodograph technique. *Wea. Forecasting*, **15**, 61–79.

——, M. R. Hjelmfelt, and P. L. Smith, 2006a: An observational examination of long-lived supercells. Part I: Characteristics, evolution, and demise. *Wea. Forecasting*, **21**, 673–688.

——, J. S. Johnson, L. J. Czepyha, J. M. Grzywacz, B. A. Klimowski, and M. R. Hjelmfelt, 2006b: An observational examination of long-lived supercells. Part II: Environmental conditions and forecasting. *Wea. Forecasting*, **21**, 689–714.

Carey, L. D., and S. A. Rutledge, 1998: Electrical and multiparameter radar observations of a severe hailstorm. *J. Geophys. Res.*, **103**, 13979–14000.

Ceperuelo, M., M. C. Llasat, L. López, E. García-Ortega, and J. L. Sánchez, 2006: Study of 11 September 2004 hailstorm event using radar identification of 2d systems and 3d cells. *Adv. Geosci*., **7**, 215–222.

——, ——, and J. L. Sánchez, 2009: Improving hail identification in the Ebro Valley region using radar observations: Probability equations and warning thresholds. *Atmos. Res.*, **93**, 474–482.

Cummins, K. L., M. J. Murphy, E. A. Bardo, W. L. Hiscox, R. B. Pyle, and A. E. Pifer, 1998: A combined TOA/MDF technology upgrade of the U.S. National Lightning Detection Network, *J. Geophys. Res.*, **103**, 9035–9044.

Deierling, W., J. Latham, W. A. Petersen, S. M. Ellis, and H. J. Christian Jr., 2005: On the relationship of thunderstorm ice hydrometeor characteristics and total lightning measurements. *Atmos. Res*., **76**, 114–126.

——, W. A. Petersen, J. Latham, S. Ellis, and H. J. Christian, Jr., 2008: The relationship between lightning activity and ice fluxes in thunderstorms. *J. Geophys. Res.*, **113**, D15210, doi:10.1029/2007JD009700.

Donavon, R. A., and K. A. Jungbluth, 2007: Evaluation of a technique for radar identification of large hail across the Upper Midwest and Central Plains of the United States. *Wea. Forecasting*, **22**, 244–254.

Doswell, C. A. III, 1987: The distinction between large-scale and mesoscale contribution to severe convection: A case study example. *Wea. Forecasting*, **2**, 3–16.

——, H. E. Brooks, and R. A. Maddox, 1996: Flash flood forecasting: An ingredients-based methodology. *Wea. Forecasting*, **11**, 560–581.

Dudhia, J., and M. W. Moncrieff, 1989: A three-dimensional numerical study of an Oklahoma squall line containing right-flank supercells. *J. Atmos. Sci.*, **46**, 3363–3391.

Edwards, R., and R. L. Thompson, 1998: Nationwide comparisons of hail size with WSR-88D vertically integrated liquid water and derived thermodynamic sounding data. *Wea. Forecasting*, **13**, 277–285.

Ek, M. B., and Coauthors, 2003: Implementation of Noah land surface model advances in the National Centers for Environmental Prediction operational mesoscale Eta model. *J. Geophys. Res.*, **108**, 8851, doi:10.1029/2002JD003296.

Emersic, C., P. L. Heinselman, D. R. MacGorman, and E. C. Bruning, 2011: Lightning activity in a hail-producing storm observed with phased-array radar. *Mon. Wea. Rev.*, **139**, 1809–1825.

Esterheld, J. M., and D. J. Giuliano, 2008: Discriminating between tornadic and non-tornadic supercells: A new hodograph technique. *Electronic J. Severe Storms Meteor.*, **3** (2), 1–50

Fehr, T., N. Dotzek, and H. Holler, 2005: Comparison of lightning activity and radar-retrieved microphysical properties in EULINOX storms, *Atmos. Res.*, **76**, 167–189.

Forbes, G. S., 1981: On the reliability of hook echoes as tornado indicators. *Mon. Wea. Rev.*, **109**, 1457–1466.

Fraile, R., A. Castro, J. L. Sánchez, J. L. Marcos, and L. López, 2001: Noteworthy C-band radar parameters of storms on hail days in northwestern Spain. *Atmos. Res.*, **59**, 41–61.

Fujita, T., 1958: Mesoanalysis of the Illinois tornadoes of 9 April 1953. *J. Meteor.*, **15**, 288–296.

García-Ortega, E., L. López, and, J. L. Sánchez, 2011: Atmospheric patterns associated with hailstorm days in the Ebro Valley, Spain. *Atmos. Res.*, **100**, 401–427.

Gayà, M., M. C. Llasat, and J. Arús, 2011: Tornadoes and waterspouts in Catalonia (1950–2009). *Nat. Haz. Earth Sys. Sci*., **11**, 1875–1883.

Goodman, S. J., R. Blakeslee, H. Christian, W. Koshak, J. Bailey, J. Hall, E. W. McCaul Jr., D. Buechler, C. Darden, J. Burks, T. Bradshaw, and P. Gatlin, 2005: The North Alabama Lightning Mapping Array: Recent severe storm observations and future prospects. *Atmos. Res.*, **76**, 423–437.

Hong, S. Y., Y. Noh, and J. Dudhia, 2006: A new vertical diffusion package with an explicit treatment of entrainment processes. *Mon. Wea. Rev.*, **134**, 2318–2341.

Johnson, E. V., and E. R. Mansell, 2006: Three dimensional lightning mapping of the central Oklahoma supercell on 26 May 2004. Preprints, *2nd Conf. on Meteorological Applications of Lightning Data*, Atlanta, GA, Amer. Meteor. Soc., 6.5.

Kain, J. S., 2004: The Kain-Fritsch convective parameterization: An update. *J. Appl. Meteor*., **43**, 170–181.

Lakshmanan, V., K. Hondl, C.K. Potvin, and D. Preignitz, 2013: An improved method for estimating radar echo-top height. *Wea. Forecasting*, **28**, 481–488.

Lang, T. J., and Coauthors, 2004: The Severe Thunderstorm Electrification and Precipitation study. *Bull. Amer. Meteor. Soc.*, **85**, 1107–1125.

Larsen, H. R., and E. J. Stansbury, 1974: Association of lightning flashes with precipitation cores extending to height 7 km. *J. Atmos. Terr. Phys.*, **36**, 1547–1553.

Latham, J., A. M. Blyth, H. J. Christian Jr., W. Deierling, and A. M. Gadian, 2004: Determination of precipitation rates and yields from lightning measurements. *J. Hydrol.*, **288**, 13–19.

Lemon, L. R., 1998: The radar "three-body scatter spike": An operational large-hail signature. *Wea. Forecasting*, **13**, 327–340.

Lojou, J. Y., and K. L. Cummins, 2006: Total lightning mapping using both VHF interferometry and time-of-arrival techniques. Preprints, *Int. Conf. on Lightning Protection*, Kanazawa, Japan, 391–396.

——, M. J. Murphy, R. L. Holle, and N. W. Demetriades, 2009: Nowcasting of thunderstorms using VHF measurements. *Lightning: Principles, Instruments and Applications*, H. D. Betz, U. Schumann, and P. Laroche, Eds., Springer, 253–270.

López, L., and J. L. Sánchez, 2009: Discriminant methods for radar detection of hail. *Atmos. Res.*, **93**, 358–368.

MacGorman, D. R., D. W. Burgess, V. Mazur, W. D. Rust, W. L. Taylor, and B. C. Johnson, 1989: Lightning rates relative to tornadic storm evolution on 22 May 1981. *J. Atmos. Sci*., **46**, 221–250.

——, W. D. Rust, P. Krehbiel, W. Rison, E. Bruning, and K. Wiens, 2005: The electrical structure of two supercell storms during STEPS. *Mon. Wea. Rev*., **133**, 2583–2607.

Metzger, E. L., and W. A. Nuss, 2013: The relationship between total cloud lightning behavior and radar-derived thunderstorm structure. *Wea. Forecasting*, **28**, 237–253.

Mlawer, E. J., S. J. Taubman, P. D. Brown, M. J. Iacono, and S. A. Clough, 1997: Radiative transfer for inhomogeneous atmosphere: RRTM, a validated correlated-k model for the longwave. *J. Geophys. Res*., **102**, 16 663–16 682.

Montanyà, J., N. Pineda, V. March, A. Illa, D. Romero, and G. Solà, 2006: Experimental evaluation of the Catalan Lightning Detection Network. Preprints, *19th International Lightning Detection Conf.*, Tucson, AZ, Vaisala, 7 pp.

——, S. Soula, and N. Pineda, 2007: A study of the total lightning activity in two hailstorms. *J. Geophys. Res*., **112**, D13118.

——, ——,——, O. van der Velde, P. Clapers, G. Solà, J. Bech., and D. Romero, 2009: Study of the total lightning activity in a hailstorm. *Atmos. Res.*, **91**, 430–437.

——, O. van der Velde, V. March, D Romero, G. Solà, and N. Pineda, 2012: High-speed video of lightning and x-ray pulses during the 2009–2010 observation campaigns in northeastern Spain. *Atmos. Res*., **117**, 91–98.

Mosier, R. M., C. Schumacher, R. E. Orville, and L. D. Carey, 2011: Radar nowcasting of cloud-to-ground lightning over Houston, Texas. *Wea. Forecasting*, **26**, 199–212.

Palencia, C., D. Giaiotti, F. Stel, A. Castro, and R. Fraile, 2010: Maximum hailstone size: Relationship with meteorological variables. *Atmos. Res.*, **96**, 256–265.

Pascual, R., 2002. Estudio de las granizadas en el llano de Lleida. Nota técnica nº 3. Centro Meteorológico Territorial de Catalunya. [In Spanish]

Pineda, N., and J. Montanyà, 2009: Lightning detection in Spain: The particular case of Catalonia. *Lightning: Principles, Instruments and Applications*, H. D. Betz, U. Schumann, and P. Laroche, Eds., Springer: 161–185.

——, M. Aran, A. Andres, M. Busto, C. Farnell, and M. Torà, 2009: Study of the September 17th 2007 severe hailstorm in Plad'Urgell. Part II: Meteorological analysis. *Tethys J. Wea. Climate West. Mediterr*., **6**, 81–100.

——, N., J. Bech, T. Rigo, and J. Montanya, 2011: A Mediterranean nocturnal heavy rainfall and tornadic event. Part II: Total lightning analysis, *Atmos. Res*., **100**, 638–648.

Ramis, C., J. Arús, J. M. López, and A. M. Mestres, 1997: Two cases of severe weather in Catalonia (Spain): An observational study. *Meteor. Appl.*, **4** , 207–217.

Rasmussen, E. N., and J. M. Straka, 1998: Variations in supercell morphology. Part I: Observations of the role of upper-level storm-relative flow. Mon. *Wea. Rev*., **126**, 2406–2421.

Rigo, T., and M. C. Llasat, 2004: A methodology for the classification of convective structures using meteorological radar: Application to heavy rainfall events on the Mediterranean coast of the Iberian Peninsula. *Nat. Hazards Earth Syst. Sci*., **4**, 59–68.

——, N. Pineda, and J. Bech, 2008. Estudi i modelització del cicle de vida de les tempestes amb tècniques de teledetecció. Notes d'estudi del Servei Meteorològic de Catalunya, 72. Barcelona, Spain, 58 pp. [In Catalan]

——, ——, and ——, 2010: Analysis of warm season thunderstorms using an object–oriented tracking method based on radar and total lightning data, *Nat. Hazards Earth Syst. Sci.*, **10**, 1881–1893.

Saunders, C. P. R., and I. M. Brooks, 1992: The effects of high liquid water content on thunderstorm charging. J. *Geophys. Res*., **97**, 671–676.

Skamarock, W. C., J. B. Klemp, J. Dudhia, D. O. Gill, D. M. Barker, W. Wang, and J. G. Powers, 2008: A description of the Advanced Research WRF Version 3. NCAR Tech. Note NCAR/TN-465+STR. [Available online at http://www2.mmm.ucar.edu/wrf/users/docs/arw_v3.pdf.]

Soula, S., Y. Seity, L. Feral, and H. Sauvageot, 2004: Cloud-to-ground lightning activity in hail-bearing storms. *J. Geophys. Res.*, **109**, d02101, doi: 10.1029/2003JD003669.

Steiger, S. M., R. E. Orville, and L. D. Carey, 2007: Total lightning signatures of thunderstorm intensity over North Texas. Part I: Supercells. *Mon. Wea. Rev.*, **135**, 3281–3302.

Tessendorf, S. A., 2009: Characteristics of lightning in supercells. *Lightning: Principles, Instruments and Applications*, H. D. Betz, U. Schumann, and P. Laroche, Eds., Springer, 161–185.

Thompson, G., R. M. Rasmussen, and K. Manning, 2004: Explicit forecasts of winter precipitation using an improved bulk microphysics scheme. Part I: Description and sensitivity analysis. *Mon. Wea. Rev.*, **132**, 519–542.

——, P. R. Field, R. M. Rasmussen, and W. D. Hall, 2008: Explicit forecasts of winter precipitation using an improved bulk microphysics scheme. Part II: Implementation of a new snow parameterization. *Mon. Wea. Rev*., **136**, 5095–5114.

Tudurı, E., R. Romero, L. López, E. Garcıa, J. L. Sánchez, and C. Ramis, 2003: The 14 July 2001 hailstorm in northeastern Spain: diagnosis of the meteorological situation. *Atmos. Res.*, **67**, 541–558.

Vaisala, 2014: IRIS, product and display manual. [Available online at ftp://ftp.sigmet.com/outgoing/manuals/IRIS_Product_and_Display_Manuals.pdf.]

Van der Velde, O. A., and J. Montanyà, 2013: Asymmetries in bidirectional leader development of lightning flashes. *J. Geophys. Res.*, **118**, 13 504–13 519.

Vasiloff, S. V., E. A. Brandes, R. P. Davies-Jones, and P. S. Ray, 1986: An investigation of the transition from multicell to supercell storms. *J. Appl. Meteor. Climatol.*, **25**, 1022–1036.

Wiens, K. C., S. A. Rutledge, and S. A. Tessendorf, 2005: The 29 June 2000 supercell observed during STEPS. Part II: Lightning and charge structure. *J. Atmos. Sci.*, **62**, 4151–4177.

Williams, E. R., and Coauthors, 1999: The behavior of total lightning activity in severe Florida thunderstorms. *Atmos. Res*., **51**, 245–265.

——, M. E. Weber, and R. E. Orville, 1989: The relationship between lightning type and convective state of thunderclouds. *J. Geophys. Res*., **94**, 13213–13220.

Yang, Y. H., and P. King, 2010: Investigating the potential of using radar echo reflectivity to nowcast cloud-to-ground lightning initiation over southern Ontario. *Wea. Forecasting*, **25**, 1235–1248.

REVIEWER COMMENTS

[Authors' responses in *blue italics.*]

REVIEWER A (Romualdo Romero):

Initial Review:

Recommendation: Accept with major revisions.

This is an interesting analysis of severe thunderstorm that affected some parts of Catalonia (NE Spain) on 5th July 2012. The special character of this storm (big hail-producing, long-lived and with some indications of supercell structure) and the number and diversity of products analyzed by the authors, make this study a valuable one for general readers and regional forecasters.

I see three major problems that in my view impede the publication of the manuscript in its current form, but I believe the authors will have the time, skills and information necessary to fix these issues. Additional (mostly technical) problems are also listed below.

Major comments:

The use of English in the document is quite poor in some phases. I provide a short list of corrections/problems in "Minor Comments", but the document as a whole should be revised and checked for the proper use of language.

We have modified substantially the document, following the reviewer indications, in order to clarify the text and make it more intelligible.

The Introduction is exceedingly long. This seems a review of the scientific literature on thunderstorms and supercells rather than an Introduction to the current case study! Authors should significantly shorten the Introduction and leave only what is essential and relevant to the case study. In some cases it is recommended to move the theoretical or observational arguments presented in the Introduction to the Results section, where these can be easily connected to the current case study. If not, the reader might be overloaded by this long introduction and, at the same time, have many difficulties in linking the July 2012 event with previous results and findings.

We have reduced this section, removing all the theory associated with the generalities of supercells and only maintaining those factors related with the region of interest.

The paper discusses at different points the meteorological situation of the event (in terms of synoptic and mesoscale environments, local/mesoscale forcings, instability, etc.) but no evidence or supporting graphical information is provided, except [then] Fig. 9. The work is entirely limited to showing radar and lightning products only. The authors must include supporting material (i.e., new figures) on the discussed meteorological aspects of the event. Some examples of these inconsistencies are listed [page and paragraph listing omitted for brevity].

Our first idea was centering only in the remote sensing (radar and lightning observations) aspects of the episode. However, and following your annotations we have added more information referent to the meteorological and thermodynamic situation, with the purpose to make more understandable the text.

[Minor comments omitted...]

Second review:

Recommendation: Accept with minor revisions.

General comment: I reviewed the new version of the manuscript and my opinion is that the authors implemented in a positive way the changes and suggestions made by the reviewers in the first round of reviews.

Regarding my particular recommendations, the manuscript is now, formally and also in content, more appealing than it was, and the reorganization made on it (especially the reduction of the very long introduction) has been very effective. Although English has been notably improved, a few problems remain (a natural aspect given the nationality of the authors; I am not an exception in this...).

We have changed [for] all the suggestions of the reviewer, and many others, considered by the other [reviewers]. However, many of the changes are not evident, because we have modified many of the paragraphs of the paper, following the suggestions of one of the reviewers.

REVIEWER B (Ronald L. Holle):

Initial Review:

Reviewer recommendation: Accept with major revisions.

General/major comments: I have reviewed the paper, "Inferring the Severity of a Long-Lived Supercell from Radar and Total Lightning Observations" by Rigo and Pineda for publication in the Electronic Journal of Severe Storms Meteorology. This is a meticulously-documented examination of supercell storms producing damaging hail using multiple datasets and analysis methods. The paper has an excellent and thorough bibliography review; in fact there are places where it is probably too extensive, as below.

I have reviewed the lightning aspects more than any other section. In general, the analyses and conclusions are consistent with existing knowledge and published results. There is one notable recent paper that needs to be added, by Metzger and Nuss (2013). That paper has conclusions with respect to the timing and location of total lightning relative to hail and other severe weather that are directly applicable to the paper under review; specific comments are listed below.

I have not corrected the English. For the most part, the meanings are understood but the phrases and grammar are rather lacking in clarity and normal usage, so it needs to be brought up to journal standards. It is, however, not a sufficiently difficult situation to reject the otherwise excellent analyses and interpretations. For that reason, I conditionally accept the paper subject to 1) including Metzger and Nuss in several places, 2) a careful reduction of some long sections, 3) addressing the list of specific issues needing attention below, and 4) accommodation of better English usage.

Metzger, E. L., and W. A. Nuss, 2013: The relationship between total cloud lightning behavior and radar-derived thunderstorm structure. *Wea. Forecasting*, **28**, 237–253.

The results relevant to the present paper are:
"..lightning jumps can be classified into severe wind, hail, or mixed-type jumps based on the behavior of various radar-based parameters…For hail-type jumps, IC flash rates increased, while CG flash rates were steady or decreased. For wind-type jumps, CG flash rates increased, while IC flash rates either increased or were steady or decreased."

A paragraph has been added concerning this reference. We agree with the reviewer about the introduction length, in fact another reviewer has also commented this point. We have reduced the introduction to what attains the current case study.

Conditions

1) *The Metzger and Nuss reference has been incorporated and cited in the text; the method they present is interesting and has been used to estimate the type of lightning jump. This result has been added into the results.*

2) *Besides the introductory part, we have reduced other sections, see further comments.*
3) *See comments on specific issues below.*
4) *English has been reviewed.*

[Minor comments omitted...]

Reduction in length: The authors are to be commended on the thoroughness of the background and literature review. There are many gems in terms of summarizing concepts that are difficult to synthesize. For example, page 3, lower left has an excellent summary of how simple parameters are not often useful for severe weather in operational meteorology. Also, page 5, left column, the long paragraph has an excellent motivation and methodology approach.

As explained previously, the introduction has been reduced, and only those important points have been moved to the corresponding section.

On the other hand, some sections are going back perhaps too far into what most readers will readily know. For example, lower right page 3 has a full history of supercells that is not used in later parts of the paper. Similarly, lower right page 5 to the start of page 6 has a full exposition on all causes of radar data errors, which are generally well known; only those relevant to the paper are needed. A careful reduction of the length of the paper should also be considered in other sections.

This section has been reduced, now it includes only those points associated with the region of interest, while the rest, if considered necessary, has been moved to other sections.

Improved English: Throughout the paper, tenses, grammar and sentence structure are very often not in standard English. There are too many minor to occasionally moderately important corrections to be made in a review.

We have made an effort to bring our "Spanish" English to standard English.

[Minor comments omitted...]

Second review:

Recommendation: Accept with minor revision.

General comment: I have reviewed the revision of the paper, "Inferring the Severity of a Long-Lived Supercell from Radar and Total Lightning Observations" by Rigo and Pineda for publication in the Electronic Journal of Severe Storms Meteorology. I have reviewed the lightning aspects more than any other section. My first review on 24 September 2014 called attention to the need to 1) include a recent paper by Metzger and Nuss in several places, 2) reduce the detail in some long sections, 3) address a list of specific issues needing attention, and 4) use better English.

For the most part, these recommendations have been taken into account, and I accept the paper in its present from. If possible, however, a few specific topics could be accommodated, as follows.

[Minor comments omitted...]

REVIEWER C (Robert A. Maddox):

[Editor's Comment: R. A. Maddox offered to examine this manuscript with the loss of a prospective third reviewer, while also assisting greatly with manuscript editing over the stages of submission and resubmission. In addition to the more formal review-level commentary and responses reproduced below, which in effect served as third review, he and the authors coordinated extensively and directly, with

oversight from the Editor, and over many months, in the details of the revision and re-writing process. As usual, minor comments are omitted.]

Initial Review:

Reviewer recommendation: Accept with major revisions.

Major comments: **I**ntroduction: This section is far too long and needs to be boiled down to a simple discussion of the region and its thunderstorms and severe weather and their economic importance. A long review of various aspects of severe thunderstorms and lightning detection/storm flash characteristics is not really needed for EJSSM readers. But in contrast, a better figure(s) are needed for the EJSSM reader to have a clearer grasp of exactly where the region of interest (ROI) is—breaking Fig. 1 into two separate figures might help. The first figure could show the geographic regions with key locations that will be referred to identified. Terrain and identification of ranges and plains could go on this figure also. The second figure then could show the details and locations of the observing systems as per the two current tiny inserts.

VIL is first mentioned on p. 2 but without a reference regarding how it is being calculated for these 5-cm radars. Reference needed and a statement about the threshold above which dBZ is not used in the VIL calculation.

We have suppressed all the theory [discussion] in respect to supercells. Figure 1 has been modified, according to your suggestions.

Analysis of the episode: I would certainly like to see a bit of explanation here of the synoptic setting – this is particularly important since this area is not familiar to most EJSSM readers. Why did the ESTOFEX team forecast severe convection a day ahead of time? It would be important to show a skewT plot of the most relevant nearby sounding for 1200 UTC on the day of the storms. The reader is left in the dark regarding the thermodynamics of the event, except for the mention of CAPE at Barcelona.

[Minor figure comments omitted...]

Important questions: 1) did the left-moving cell-1 storm originate with a storm split as is often (usually?) the case? 2) Was cell 2 also a supercell? 3) Why haven't the authors used the Doppler velocity fields to demonstrate which storms were and were not supercells (major problem)?

We are agreeing with appreciation on respect to the meteorological conditions, and have introduced some paragraphs referring to the synoptic conditions at low and upper levels, and to the thermodynamic conditions. These paragraphs have been added in a new subsection titled "Atmospheric conditions".

Answers to the important questions:

1) Effectively, the cell#1 birth from a split of a previous cell (it is better commented in the growing phase section);
2) We will try to answer questions (2) and (3) in the next section. However, we can advance that cell #2 probably was also a supercell (but is not evident as cell #1), and we have added a figure of Doppler wind.

The most important issue of this section is why are the authors trying to infer whether this was a supercell when they have Doppler radar data? Other key questions are: Was the mesocyclone rotating cyclonically or anticyclonically? Where was the mesocyclone located relative to the reflectivity core and movement of the supercell?

The main problem of the SMC radars for the Doppler wind, and mainly for the CDV radar (the closer one to the thunderstorm) is in the coherence of the field caused by the unfolded signals. We have tried to solve your questions with [a figure that] shows cyclonic rotation at mid-levels, and axisymmetric convergent flow at lower CAPPI, maybe associated with the downburst that was detected by automatic weather stations at

surface. The mesocyclone was located in the rear right flank, in relation to the reflectivity core and movement of the supercell.

[former] Fig. 11: This figure needs substantial work. The idealized hodograph of Chisholm and Renick is not relevant to this study, although a hodograph from a case study of a left-moving supercell would be relevant. The hodograph from Zaragoza needs considerable additional explanation and analysis. Further, if hodograph to be used is from Zaragoza, the thermodynamics of that sounding need to be shown and the CAPE at Barcelona is not particularly relevant.

Legends: What are the units of speed for top hodograph? What are the heights of the points shown? Storm motion vector shown seems to be for a right moving storm—why? The technique of Bunkers et al. as per:

Bunkers, M. J., B. A. Klimowski, J. W. Zeitler, R. L. Thompson, and M. L. Weisman, 2000: Predicting supercell motion using a new hodograph technique. *Wea. Forecasting*, **15**, 61–79.

...should be applied to the Zaragoza hodograph and the motion vectors for both right and left moving supercells shown.

As has been shown in Fig. 12, this part has been increased, introducing the hodographs for the radiosonde of Barcelona and Zaragoza, and also the estimated by the WRF model for the ROI. For all of them, the Bunkers et al (2000) technique has been applied in order to get the LM and RM. The thermodynamics values are introduced in section 3a, for the two radiosondes.

Second review:

Recommendation: Accept with major revisions.

Major comments: First: I want to commend the authors for their substantial work done to clarify their study results in response to the first reviews. Many improvements have been made, and I have read carefully their response to my initial comments.

Thank you very much. The comments of reviewers like you are always well-received and they have helped a lot to understand better some dark points in our research and improve our work a lot.

Second: Regarding the authors' question to me regarding VIL, I think that the best way to introduce findings related to VIL is just to comment: "VIL was calculated as per (REF, date)", and leave it simple, but allow the interested reader to go to a reference to see how you calculated VIL. Remember that EJSSM readers will be most familiar with severe storm signatures that have been developed from 10-cm radar data.

We don't use a special technique, if not, the standard product given by the commercial software implemented in our radar network (Interactive Radar Information System, IRIS, from SIGMET-Vaisala). Then, we understand that in our case, giving the reference of the IRIS products manual is enough or it doesn't?

Third: Although the authors have made substantial changes and improvements to the revised paper, I still find parts of it very hard to follow. Much of this is due to the continuing need for substantial editing of the English. However, there are a number of technical issues remaining, and I will focus my comments on these. I will leave most of the lightning aspects of the paper to the other reviewers. I have grouped my comments relative to three aspects of the event and your study. I am going to present many of my comments and concerns by focusing on the figures.

Fig. 1: I still think that this figure would be most effective if it were presented as two separate figures—top portion in section 1 and bottom portion in section 2. The topography of the study area is much more complex than I had realized. The top part of figure really does not convey to the reader the following aspects of the setting: 1) moderate mountains cover a large area to the west of the Lleida Plain; 2) the terrain slopes strongly upward to the east of the Plain into the high Pyrenees Mountains; 3) there is a small

range of mountains (~500–1000 m elevation) between Barcelona and the Plain; and 4) the Plain is very low elevation and is open to the Mediterranean through the narrow river valley that is southwest of the LMI radar site (note that the LMI radar appears to be located within the coastal mountains, although this is not clear from the figures nor from a terrain map I found easily online).

One of the main problems for the meteorologists in Catalonia (and other parts of the Mediterranean Region) is the very complex topography. We have tried to include in the text your suggestions. However, it is complicated to show all the complexities of the topography for the whole region. Because we understand that it is necessary to show to the readers the situation of Catalonia in Europe, it is also possible to add another map for showing the complexity of the topography centered in the region of study.

Re: automated weather stations: The authors mention a network of surface stations in the second paragraph and then later in the text regarding winds and a downburst. The data from some of these automated stations would add much to the study by showing what surface conditions were immediately ahead of the severe thunderstorm (cell #1). This is important since low levels in the Barcelona sounding represent the coastal region, which appears isolated from the Plain by the mountains mentioned above. Further, the low-levels of the Zaragoza sounding appear to sample the environment behind a cold front that is moving across Spain ahead of the 500-hPa trough.

We have added a text introducing the Automatic Weather Stations network of the SMC (XEMA).

This [p. 3 text] continues to be confusing with the mention of windmills and communication antennas. The authors conclude that there were no sampling problems of significance during this event and it should be fine for them just to state this without mention of things that did not impact their study. There are, of course, problems inherent in the 5-cm radar observations with attenuation being the major issue, but authors in their response also mention problems in unfolding the velocity data (probably due to the unambiguous velocity being fairly low).

We have reduced the text, removing the part associated to possible errors, and only including those observed anomalies in the radar data during the event.

Re: the skew-T diagrams: The diagrams shown in Fig. 3 are NOT Skew-T charts but are actually Stuve diagrams. Skew-T plots for this event are available online at the Univ. of Wyoming upper-air site. The soundings pose a bit of a challenge also. The values of CAPE are not at all indicative of severe thunderstorm potential, leading me to scratch my head and wonder what was going on. My best guess is that the low-levels have much more CAPE over the Lleida Plain than do either of the nearby soundings. Resolving this issue requires careful consideration of the surface observations within the ROI.

We have replaced Stuve with skew-T.

I also note that the surface values of T and T_d are pathologically high in the soundings you show. θ_e plunges as soon as the sonde is launched. This seems to indicate that conditions within the preparation shelter/building are warmer and more moist than the external environment encountered by the sonde as soon as it leaves the launch tube. It is necessary to ignore the non-representative surface values and to assess the thermodynamics using layer means (as is done at the Univ. of Wyoming site).

[Editor's Note: The reviewer also sent me a photo of the RAOB launch facility at University of Barcelona; the balloons are launched from the inside out through a tube. It appears as if the authors either should just use the University of Wyoming sounding archive as suggested (with layer means), or preferably, modify the soundings using their own software with the most representative possible surface observation—either at Barcelona airport (which is near sea level) or perhaps somewhere on the Plain in an environment not affected by the storms (if available).]

We have changed the part of this analysis, generating a new sounding, combining the information from the WRF model (low levels) and the soundings from Barcelona and Zaragoza (mid and top levels). We have also changed the thermodynamic values, recalculating from the University of Wyoming webpage.

It appears to me that cell #1 is not a left-moving storm, but is rather moving with the approximate mean wind from about 700–400 hPa.

The cell seems to move with the wind at 3 km, mainly at the last hour. However, this time is far for the time of the hodograph. Furthermore, [there] exists a veering to the left of the mean direction of the translation of cell #1 across its life cycle.

My impression is that cell 2 was a multicell storm (one with cell components moving eastward and weakening over higher terrain), while new cells formed on the right rear flank of the cells. This leads to an extreme, apparent movement to the right of the winds, but this is a track of the propagation component related to the multiple cells. Perhaps the propagation was outflow driven and toward the most unstable, low-level air? It is puzzling as to why most cells had westerly tracks.

Cell #2 was moving in a terrain with a high slope, and influenced by the Pyrenees (at the left of the thunderstorm, according to its motion). Then, the topography could play an important role in the anomalous propagation of this thunderstorm, at is explained in the new text, and following your suggestions.

Figure 16: This graphic shows Doppler velocities at the same time as the previous figure. The cross section in bottom panel needs to show heights of 2 and 6 km for proper interpretation (i.e., the velocity field along A–B at 2 and 6 km should agree with the velocity fields at those heights in the cross section—there are currently discrepancies). For example, there are two distinct inbound (blue) areas at ~6 km shown in the cross section that don't seem obvious on the top panel. At 2 km there is a strong outbound area (red) that is apparent on middle panel, but south of line A–-B. Thus, there appear to be detail issues here that need to be corrected.

The strong outbound velocities at 2 km (resulting in a line of convergence) are not a typical downburst signature. But there are certainly deep and strong, outbound radial velocities occurring. At 6 km the authors have identified an area of cyclonic circulation (white dots), but this is quite weak in comparison to the very strong, anticyclonic, mesocyclone signature located at the leading edge of the cell. This signature is perhaps strong enough to be called a TVS? Another mystery presents itself here: why is there no anticyclonic hook echo associated with this apparently intense circulation?

After a hard analysis, and thanks to the collaboration of P. Altube and Dr. Bech, we have found some figures that could help to show better some evidences in the Doppler velocity fields. In any case, the low quality of the data, probably associated to the strong shear produced by the cell #1, has not helped to identify easily the rotation of the thunderstorm. In any case, it seems moderately clear the presence of the anti-cyclonic rotation at mid-levels, according to the panels presented in Fig. 17, which is the result of the analysis of many images of CAPPIs and PPIs.

[Minor comments omitted.]